Ore Geology Reviews 73 (2016) 354–373

Contents lists available at ScienceDirect

Ore Geology Reviews

journal homepage: www.elsevier.com/locate/oregeorev

Geological and geochemical constraints on the genesis of the Huachanggou gold deposit, western Qinling region, Central China

Chonghao Liu [a,b], Jiajun Liu [a,b,*], Emmanuel John M. Carranza [c], Longbo Yang [d], Jianping Wang [a,b], Degao Zhai [a,b], Yinhong Wang [a,b], Jie Wu [a,b], Hongzhang Dai [a,b]

[a] State Key Laboratory of Geological Processes and Mineral Resources, China University of Geosciences, Beijing 100083, People's Republic of China
[b] School of Earth Sciences, China University of Geosciences (Beijing), Beijing 100083, People's Republic of China
[c] School of Earth and Environmental Sciences, James Cook University, Townsville, QLD 4811, Australia
[d] Department of Earth & Planetary Sciences, McGill University, Montreal H3A2A7, Canada

ARTICLE INFO

Article history:
Received 23 March 2014
Received in revised form 3 August 2015
Accepted 6 August 2015
Available online 14 August 2015

Keywords:
Huachanggou gold deposit
Qinling orogen
Geology
Geochemistry
Ore genesis

ABSTRACT

The Huachanggou gold deposit is located in Lueyang County, Shaanxi Province, central China; it is situated in the Mian–Lue sutural zone in the western Qinling Orogen and controlled by a WNW-striking ductile shear zone. The ore deposit is developed in spilite, limestone and phyllite in the Middle–Lower Devonian Sanhekou Group, and the wall rocks show evidence of deformation. Pyrite is the main gold-bearing mineral, and the native gold is either visible or microscopic.

The Huachanggou gold deposit is considered to be an orogenic gold deposit controlled by a ductile shear zone related to the Indosinian Qinling orogenic event. The ores show a strong enrichment in Au, Ag and As but exhibit a simple assemblage of Au and Ag that are strongly correlated together. Gold was deposited from a moderate to low salinity, salt solution–CO_2 hydrothermal fluid at medium temperature. Variations in S, Pb, C, and O isotopic composition indicate that the sulfur was derived from the reduction of seawater sulfate in the wall rocks; the lead was derived mainly from the wall rocks; the carbon was derived from the dissolution of marine carbonate. The variations in H and O isotopic composition indicate that the ore-forming fluids were derived originally from metamorphic fluid with meteoric water mixing in later stages. Au migrated mainly in the form of $Au(HS)_2^-$ to form the deposit. Boiling of the fluid triggered the precipitation of the metal sulfides that contain the gold.

1. Introduction

The Qinling Orogen, in central China, separates the North China Block (NCB) from the South China Block (SCB) and links the Kunlun Orogen to the west with the Dabie–Sulu Orogen to the east (Fig. 1a). This region is an important tectonic domain in China, and the gold metallogeny has drawn international attention (e.g., Lerch et al., 1995; Webb et al., 1999; Ratschbacher et al., 2003; Luo et al., 2012; Zeng et al., 2012; Goldfarb et al., 2014). The western Qinling region is one of the most important gold producing regions in China. Over 50 gold deposits are distributed within the east-trending thrust and sutural zones in this region (Fig. 1b). The deposits are typical orogenic, Carlin-type and Carlin-like gold deposits (Hu et al., 2002; Mao et al., 2002, 2005, 2012; Chen et al., 2004; Liu et al., 2015a).

In the western Qinling region, most of the orogenic gold deposits occur between the Shang–Dan suture and Fengxian–Zhen'an fault, but some are located along the Mian–Lue suture; these deposits are confined to WNW-trending brittle–ductile shear zones in the Devonian and Carboniferous greenschist-facies metasedimentary rocks which were strongly deformed and metamorphosed during the Indosinian collision between the North China Block and the South China Block (Mao et al., 2002; Chen et al., 2004; Liu et al., 2015a). Phanerozoic collisional orogenic event produced the orogenic gold deposits of the western Qinling region (Feng et al., 2002, 2003; Chen et al., 2004; Zhu et al., 2009, 2010; Dong et al., 2011). The geological characteristics of orogenic gold deposits in this region, which include the Baguamiao, Ma'anqiao and Liziyuan orogenic gold deposits, include compressional to transpressional structures, deformed and variably metamorphosed host rocks, and moderate–low salinity, CO_2-rich, neutral to slightly alkaline fluids (Mao et al., 2002; Chen et al., 2004; Wen et al., 2007; Yang et al., 2012a; Liu et al., 2015a). These characteristics are similar to those of many orogenic gold deposits throughout the world (e.g., Groves et al., 1998, 2003; Chen et al., 2007; Goldfarb et al., 2014).

The Huachanggou gold deposit is located in Lueyang County, about 300 km southwest of Xi'an in Shaanxi Province, China. It has a contained gold reserve of about 10 tonnes with a grade of 2–10 g/t (Li et al., 2014). The deposit is controlled by a ductile–brittle shear zone along the Mian–Lue sutural zone (Fig. 1b). Three ore zones (termed ore zones I, II and III)

* Corresponding author at: State Key Laboratory of Geological Processes and Mineral Resources, China University of Geosciences, Beijing 100083, People's Republic of China.
E-mail address: liujiajun@cugb.edu.cn (J. Liu).

http://dx.doi.org/10.1016/j.oregeorev.2015.08.002
0169-1368/

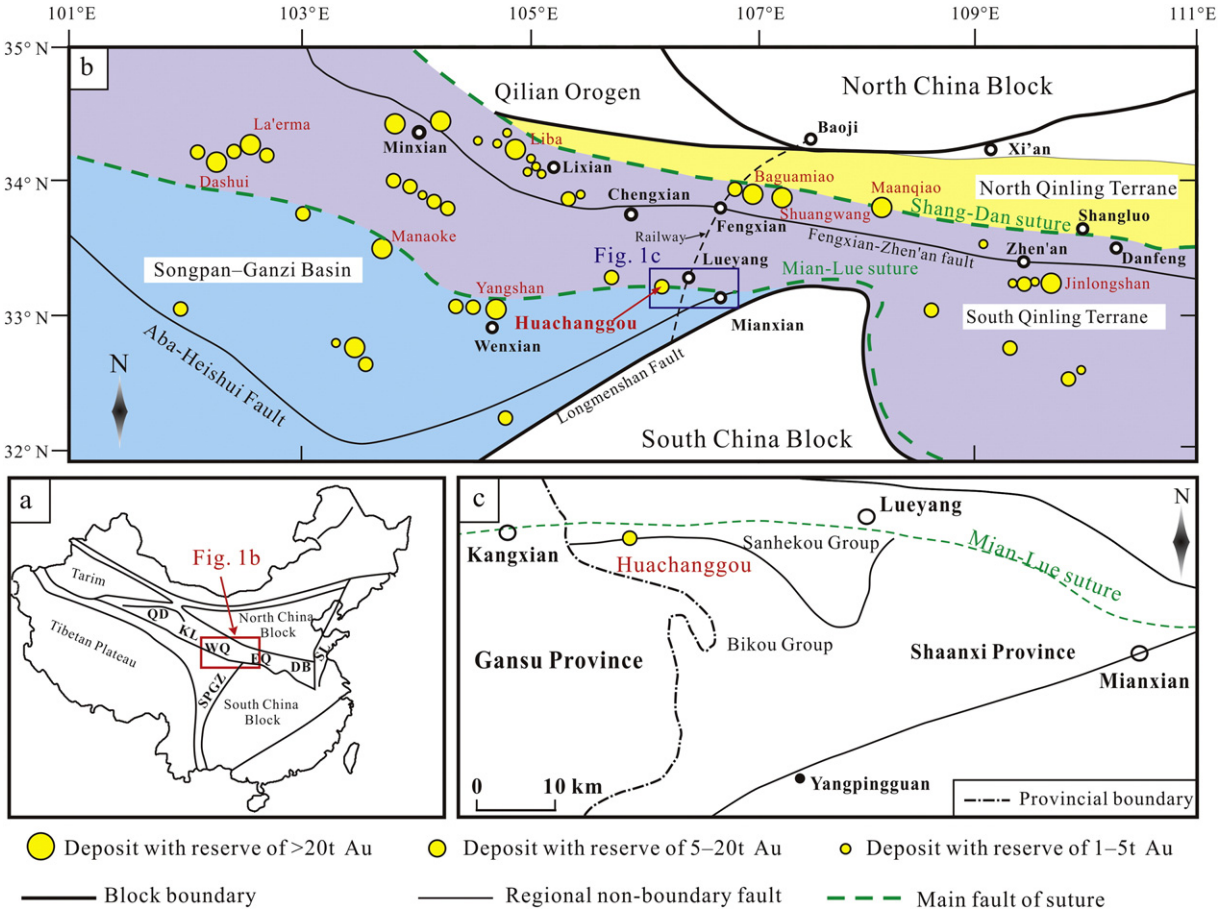

Fig. 1. Sketch geological maps of the Huachanggou gold deposit. a. Simplified map of China, showing major tectonic units of China (after Zheng et al., 2010). b. Sketch geological map of the Qinling Orogen, showing the location of gold deposits in this area (modified after Chen et al., 2004; Zeng et al., 2012). c. Sketch regional geological map of the Huachanggou gold deposit (modified after Wei et al., 2000). QD = Qaidam; KL = Kunlun Shan belt; WQ = West Qinling; EQ = East Qinling; DB = Dabie belt; SL = Sulu belt; SPGZ = Songpan–Ganzi terrane.

comprise the Huachanggou mine, of which zone I has been the main focus of previous studies where evidenced was presented for a hydrothermal origin of the gold in the altered spilite (e.g., Bai, 1996a,b; Wei et al., 2000; Li and Tai, 2007). Only the orebodies in ore zone I are hosted in spilite; limestone and phyllite host the ore in zones II and III.

In this paper, we describe aspects of the geology of the Huachanggou gold deposit, including the structural framework, ore petrology, alteration, and the style of mineralization. We present data on the pyroelectricial property of pyrite, the composition of the ore-forming elements, together with fluid inclusion and stable isotope data (S, Pb, H, O, and C). We propose a model for the source of the ore-forming fluid and metals, the evolution of these fluids, and the mechanism of mineralization.

2. Regional geology

The Qinling Orogen is divided by three major tectonic zones termed the Shang–Dan suture, the Fengxian–Zhen'an fault and the Mian–Lue suture (Fig. 1b). The Paleozoic Shang–Dan suture separates the North Qinling Terrane (NQT) from the South Qinling Terrane (SQT) (Dong et al., 2011). The NQT, which hosts minor gold mineralization, was accreted to the NCB along the Shang–Dan suture (Mao et al., 2002; Zeng et al., 2012). Geographically, the boundary between the western and eastern Qinling regions is approximated by the Baoji–Fengxian–Lueyang Railway (a part of Baoji–Chengdu Railway) (Fig. 1b; Zheng et al., 2010; Zeng et al., 2012).

The Mian–Lue oceanic basin opened up within the northern margin of the SCB since Devonian and separated the SQT from the SCB (Yin and Nie, 1996; Zhang et al., 2007a; Zheng et al., 2010). The Mian–Lue oceanic crust underwent northward-facing subduction beneath the SQT from Permian to Early Triassic (Dong et al., 2011). After the extinction of the Mian–Lue oceanic crust, the collision between the SCB and SQT took place along the Mian–Lue suture in Middle–Late Triassic (Zhai et al., 1998; Meng and Zhang, 1999, 2000; Jiang et al., 2010).

The Huachanggou gold deposit is located in the middle section of the Mian–Lue sutural zone (Wei et al., 2000). It is generally accepted that an important period of gold-formation took place in the western Qinling region during Late Triassic after the closure of the Mian–Lue Ocean (Mao et al., 2002; Chen et al., 2004). A fuchsite K–Ar age for the gold-formation of the Huachanggou gold deposit is 215 ± 0.5 Ma (Bai, 1996a,b). A number of zircon SHRIMP U–Pb ages of the quartz veins, which were formed during the main mineralization stage, range from 199 to 230 Ma (Lin et al., 2011). These age data of the Huachanggou gold deposit are consistent with the mineralization ages of other major gold deposits of the western Qinling region (233–197 Ma; Liu et al., 2015a), and these ages are close to the time of collision along the Mian–Lue suture (Jiang et al., 2010; Dong et al., 2011). Metavolcanic rocks from the Heigouxia Valley, which was produced by the subduction of the Mian–Lue oceanic crust, have yield a Sm–Nd isochron age of 242 ± 21 Ma and a Rb–Sr isotopic age of 221 ± 13 Ma which is believed to represent the time of metamorphism (Li et al., 1996b). The granulite mineral samples from the central segment of the Mian–Lue suture yielded a Sm–Nd isochron age of 206 ± 55 Ma

and a biotite $^{40}Ar/^{39}Ar$ plateau age of 199.7 ± 1.7 Ma (Zhang et al., 2002). We conclude that the Late Triassic age (215 ± 0.5 Ma; Bai, 1996a,b) is acceptable for the Huachanggou mineralizing event, and the gold-formation was related to Indosinian orogenic event in the Qinling Orogen.

3. Geology of the Huachanggou gold deposit

3.1. Structural framework

The Huachanggou gold-forming event involved structural control by a complex large-scale regional ductile shear zone and multistage faults (Fig. 2; Wei et al., 2000, 2005; Zhang et al., 2007b). The ductile shear zone is over 15 km in length and ~2 km in width and covers the whole district where mineralization is developed from WNW to ESE (Fig. 2). The deformed wall rocks show evidence of strong extrusion force (Fig. 3a) and exhibit asymmetric shear fold which indicates a dextral sense of shear (Fig. 3b), strongly foliated spilite (Fig. 3c) and stretched quartz veins as boudinage (Fig. 3d).

Two phases of faulting are recognized. Earlier WNW-striking faults form the boundaries between different strata along wavy fault planes, e.g., the boundaries between Bikou Group and Sanhekou Group (F_3 in Fig. 2) and between different layers of the Sanhekou Group (F_6 in Fig. 2). Later WNW-striking fault (F_2 in Fig. 2) and NE-striking fault (F_7 in Fig. 2) are shear faults which were formed after the formation of gold mineralization, and they are characterized by a straight fault plane (Wei et al., 2005).

3.2. Host rocks

The Huachanggou gold deposit is located about 4 km south of the Kang–Lue–Mian deep fault zone, and it is a part of the Mian–Lue sutural zone in the Qinling Orogen (Fig. 1c). The Sanhekou Group hosts the gold mineralization, and it belongs to the Kangxian–Lueyang Variscan fold zone (Fig. 1c; Liu et al., 2013a; Wei et al., 2000, 2005). The Bikou Group to the south of the Sanhekou Group consists of tuffs and spilite lenses which belong to the Caledonian-aged Motianling fold zone.

The Middle–Lower Devonian Sanhekou Group comprises five layers (Fig. 2); viz: 1. Silty sericite phyllite, calcareous phyllite and metamorphic quartz sandstone. 2. Bedded microcrystalline limestone, argillaceous limestone and bioclastic limestone. 3. Tuffaceous sericite phyllite, tuffaceous slate and lenticular spilite. 4. Calcareous phyllite, silty sericite phyllite and metamorphic quartz sandstone. 5. Bedded crystalline limestone and quartz sandstone. The spilite is mostly red purple and khaki in color (Fig. 4a) and occurs in the form of lenses. The spilite lenses exhibit a similar strike and dip to that of the other strata.

3.3. Ore bodies

There are three major ore zones (termed ore zones I, II and III) in the Huachanggou gold deposit. The existing mining districts of the three ore zones are from exploration lines 0 to 44, from lines 170 to 230, and from lines 30 to 80, respectively (Fig. 2).

Ore zone I is the largest one among the three ore zones and is located in the western part of the district, extending from northern Zhaiziwan

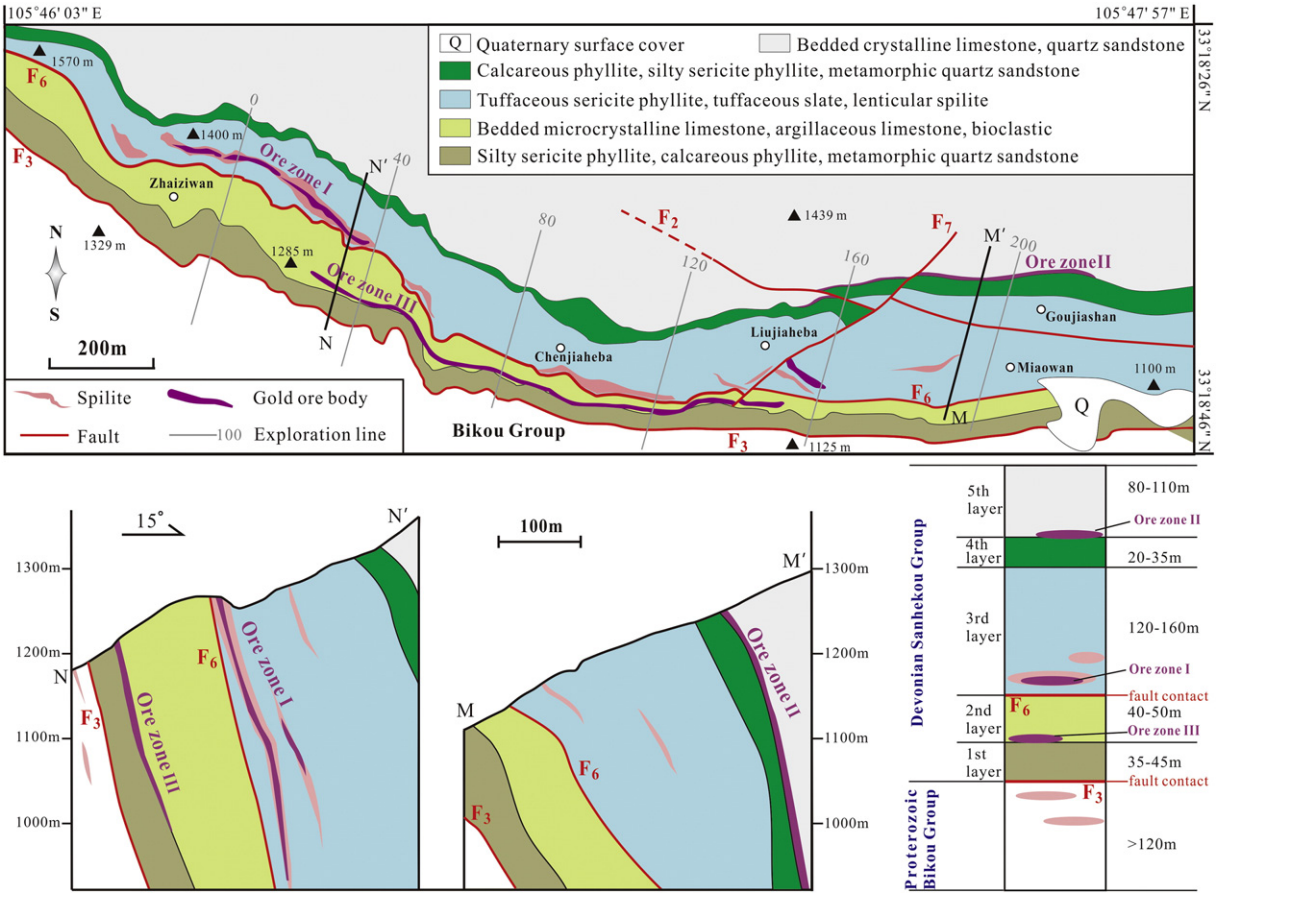

Fig. 2. Geological map of the Huachanggou gold deposit (after Liu et al., 2013a). The left bottom insert shows the geological cross sections along lines N–N′ and M–M′; the right bottom insert shows the regional strata sequences and contact relationships (data after Li and Tai, 2007).

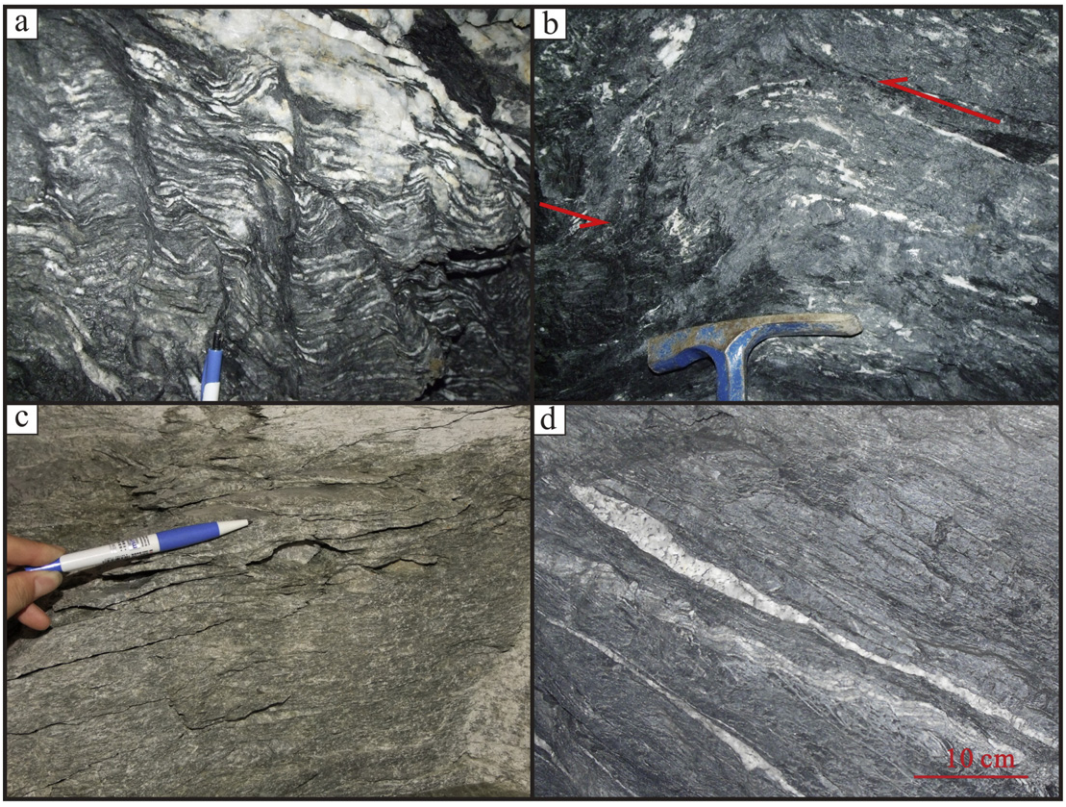

Fig. 3. Structural features of ductile shear zone in the Huachanggou gold deposit. a. Shear folds indicate strong extrusion force. b. Asymmetric shear fold indicates a dextral sense of shear. c. Strongly foliated spilite. d. Stretched quartz veins as boudinage.

to eastern Chenjiaheba for more than 2 km (Fig. 2). Altered spilite hosts ore zone I gold mineralization. Five NW-striking orebodies exhibit north-dipping dips of 55–65°, and the gold grade ranges from 2 to 6 g/t and locally reaches 36.8 g/t (Table 1).

Ore zone II is located in the northeast part of the district, extending from northern Liujiaheba to Goujiashan for about 1.8 km (Fig. 2). Bedded crystalline limestone and silty sericite phyllite is the host of the gold orebodies which dip to the north at an angle of 60–80°. The gold grade varies from 2 to 10 g/t and locally reaches 38.2 g/t (Table 1).

Ore zone III is located in the southern part of the district (Fig. 2), extending from southeastern Zhaiziwan to southern Liujiaheba for about 2 km. Microcrystalline limestone and silty sericite phyllite is the host of WNW-trending orebodies which dip to the north at 40–75°. The gold grade varies from 2 to 8 g/t and locally reaches 30.7 g/t (Table 1).

3.4. Ore mineralogy

Ores in the Huachanggou gold deposit can be divided into altered spilite-type and carbonate–quartz vein type.

The altered spilite type ores occur in ore zone I and exhibit block structure (Fig. 4a). The majority of metallic minerals are pyrite, chalcopyrite and native gold, and the gangue minerals are quartz, albite, calcite and ankerite. Pyrite occurs as disseminations (Fig. 4b, c)

The carbonate–quartz vein type ores occur in ore zones II and III which have higher gold grade and are characterized by banded quartz veins (Fig. 4d, g). The majority of metallic minerals are pyrite, chalcopyrite and native gold, and minor galena and sphalerite (Fig. 4i). The gangue minerals are quartz, albite, calcite and ankerite. Pyrite occurs as disseminations (Fig. 4e, h).

The major gold-bearing mineral in the deposit is pyrite. Native gold in the deposit is both visible and microscopic. Visible gold occurs mainly in quartz veins with size of about 3 mm (Fig. 5a, b). Microscopic gold occurs mainly in the form of inter-particle gold (Fig. 5c), minor inclusion gold (Fig. 5d) and fissure gold (Fig. 5e, f) (Liu et al., 2013b).

3.5. Wall rock alterations and hydrothermal events

Gold mineralization in the Huachanggou gold deposit is associated with intense hydrothermal alteration, which includes silicification, carbonation, sericitization, chloritization and epidotization. Silicification shows close relationship with mineralization and occurs widely in the form of quartz veinlets which infilled the schistosity and fissures of the wall rocks (Fig. 4b, e). Carbonation was developed after silicification and generally occurs in the form of pyrite–quartz–carbonate veins. Gold mineralization generally occurs within the mineralized areas where silicification is most intense and pyrite is disseminated in the silicified haloes (Fig. 4e).

The gold-forming event in the Huachanggou deposit underwent a period of hydrothermal mineralization and then supergene oxidation. Based on the relationships between the ore veins, the mineral assemblages and the paragenetic sequence (Table 2), three stages of hydrothermal mineralization can be identified (Zhou et al., 2011a):

1. Stage I is marked by the occurrence of quartz–ankerite–pyrite veins along stratigraphic bedding planes (Fig. 6a) and is characterized by idiomorphic cubic pyrite (>2 mm in size) which imparts a dark yellow hue to the rock and occurs as disseminations (Fig. 6a, b).
2. Stage II (the main stage) is marked by polymetallic sulfide–quartz–carbonate veins and is characterized by pyrite, native gold, chalcopyrite and galena. The veins occur in the form of fillings along fissures. Hypidiomorphic–allotriomorphic pyrite (<0.8 mm in size) imparts a light yellow hue to the rock and occurs as disseminations (Fig. 6c, d).

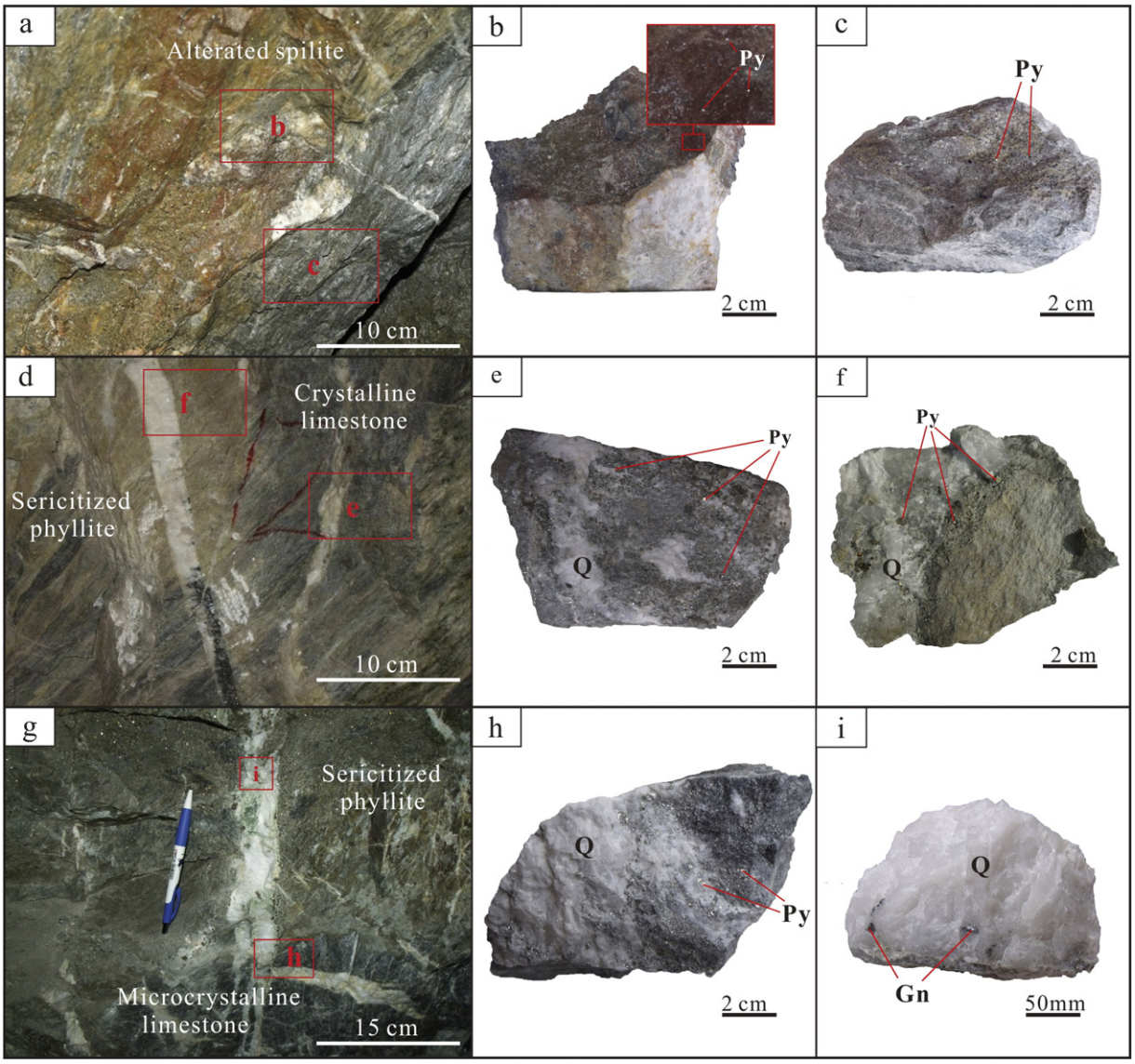

Fig. 4. Photographs of ores from ore zones I (a, b, c), II (d, e, f) and III (g, h, i) in the Huachanggou gold deposit. a. Altered spilite exposed in the tunnel of ore zone I. b and c. Altered spilite type ore, with pyrite occurring as disseminations. d. Limestone and phyllite exposed in the tunnel of ore zone II. e. Carbonate–quartz vein type ore, with pyrite occurring as disseminations. f. Carbonate–quartz vein type ore, and pyrite are distributed in the form of vein. g. Limestone and phyllite exposed in the tunnel of ore zone III. h. Carbonate–quartz vein type ore from microcrystalline limestone, with pyrite occurring as disseminations. i. Galena in quartz vein from microcrystalline limestone. Q = quartz; Py = pyrite; Gn = galena.

3. Stage III is marked by quartz–carbonate veins which cross-cut the strata and the early formed quartz veins (Fig. 6e, f). Small amounts of pyrite occur in quartz–calcite veins (Fig. 6f). The main difference between stage II and stages I and III is the development of polymetallic sulfides in stage II. And the main difference between stage I and stage III is the occurrence of abundant calcite in stage III veins.

Table 1
Geology and mineralogy of the Huachanggou gold deposit.

Ore zone	Scale	Host	Major alteration	Grade	Ore mineralogy	Gangue mineralogy
I	>2 km length; 3–15 m thickness	$D_{1-2}sh^{1c}$ alternated spilite	Silicification, chloritization, carbonatation, epidotization	2–6 g/t, locally 36.8 g/t,	Pyrite, chalcopyrite, galena, native gold	Quartz, albite, calcite, dolomite
II	1.8 km length; 0.5–1.2 m thickness	$D_{1-2}sh^{2a}$ silty sericitized phyllite $D_{1-2}sh^{2b}$ bedded crystalline limestone	Phyllitization, silicification, sericitization, carbonatation	2–10 g/t, locally 38.2 g/t	Pyrite, chalcopyrite, galena, native gold	Quartz, albite, ankerite, calcite, dolomite
III	2.6 km length; 0.3–0.8 m thickness	$D_{1-2}sh^{1a}$ silty sericitized phyllite $D_{1-2}sh^{1b}$ microcrystalline limestone	Phyllitization, silicification, sericitization, carbonatation	2 to 8 g/t, locally 30.7 g/t	Pyrite, chalcopyrite, galena, native gold	Quartz, albite, calcite, ankerite, dolomite

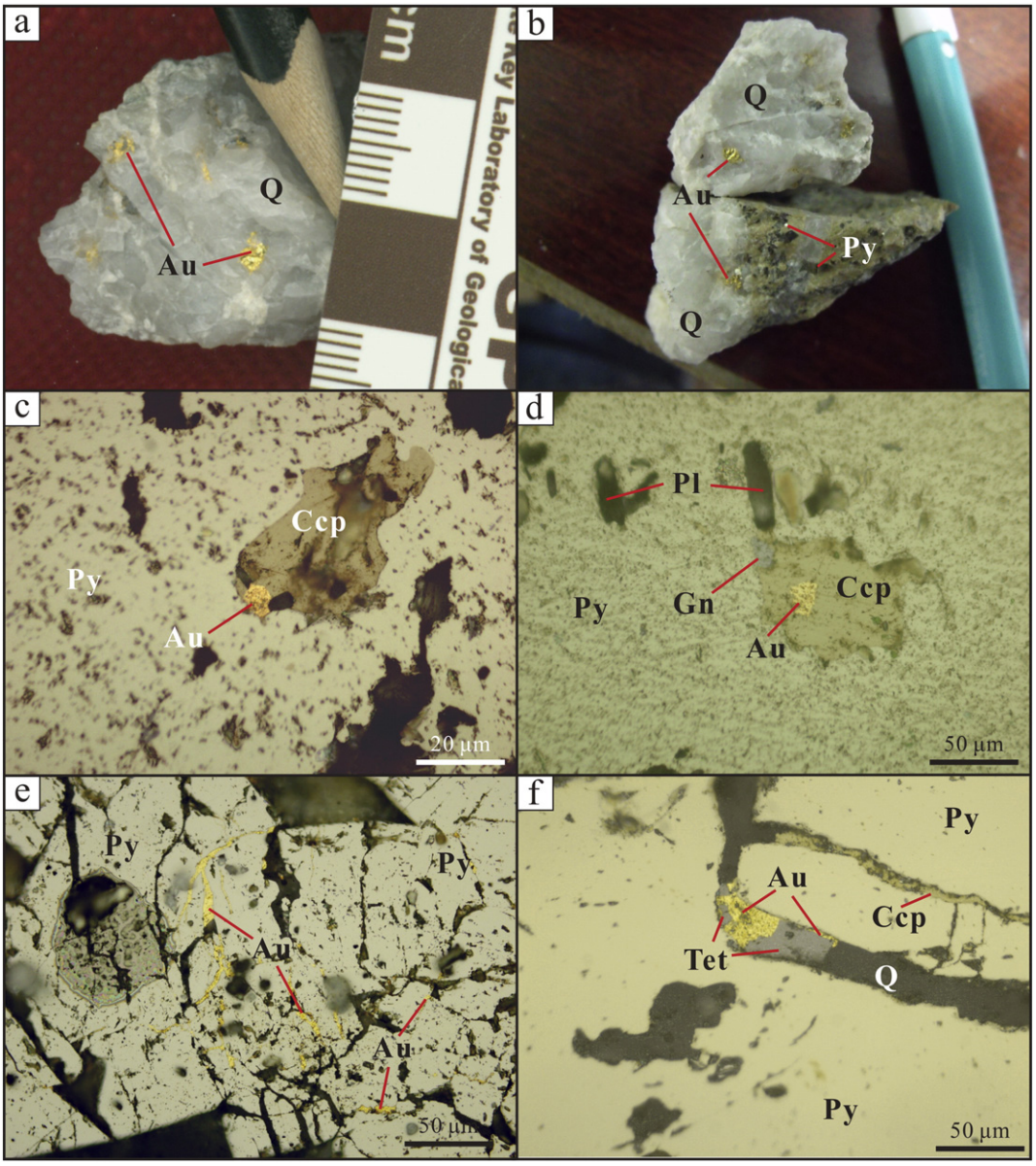

Fig. 5. Photographs of native gold and other minerals in ores from the Huachanggou gold deposit. All microphotographs are in reflected light. a. Visible gold in white quartz vein. b. Visible gold intergrown with sulfides in white quartz vein. c. Interparticle gold within the sealed fractures of pyrite and chalcopyrite. d. Inclusion gold within chalcopyrite. e and f. Fissure gold within the fractures of pyrite. Au = native gold; Py = pyrite; Ccp = Chalcopyrite; Tet = tetrahedrite; Q = quartz; Pl = plagioclase.

4. Sampling and analytical methods

The locations of samples in this study are shown in Fig. 7. Sampling was undertaken to meet the following conditions: (1) to minimize the effect of weathering, (2) to ensure that materials were available from both hanging wall and footwall environments, and (3) to obtain representative examples of each type of ore and wall rock.

The concentration of Au was analyzed by FAAS (flameless atomic absorption spectrometry analyses), Ag by ES (emission spectrometry), As by HG-AFS (hydride generation atomic fluorescence spectrometry), Hg by CV-AFS (cold vapor atomic fluorescence spectrometry), Mn by XRFS (X-ray fluorescence spectrometry), and other elements by ICP-MS (inductively coupled plasma mass spectrometry) at The Institute of Geophysical and Geochemical Exploration, Chinese Academy of Geological Science, Langfang, China.

Pyroelectric property analysis of pyrite was carried out using a Yinghuazhi YHZ-1106 pyroelectricity apparatus at the laboratory of The Teaching and Research Section of Mineral Deposit and Exploration, China University of Geosciences, Beijing, China. The activation temperature was set at 60 °C (Hu, 2001; Shen et al., 2013).

Microthermometric analysis of fluid inclusions was carried out using a Linkam THMSG 600 heating–freezing stage at The State Key Laboratory of Geological Processes and Mineral Resources, China University of Geosciences, Beijing, China.

The composition of fluid inclusions was analyzed using a Shimadzu GC2010 gas chromatograph and a Shimadzu HIC-SP Super ion chromatograph by a thermal decrepitation method at The Mineral Resources Research Institute, Chinese Academy of Geological Sciences, Beijing, China.

Sulfur and lead isotope analyses of pyrite were carried out using a Finnigan MAT-253 mass spectrometer by the procedure outlined by Glesemann et al. (1994) at The Beijing Research Institute of Uranium Geology, Beijing, China.

Hydrogen and oxygen isotope analysis of quartz were carried out using a MAT-253 mass spectrometer by the method of Clayton and Mayeda (1963) and Coleman et al. (1982) at The National Research

Table 2
Paragenetic sequence of main minerals in the Huachanggou gold deposit.

Periods and stages of mineralization	Hydrothermal mineralization			Supergenetic oxidation
	Stage I	Stage II	Stage III	
Quartz	▬	▬	▬	
Pyrite	▬	▬	▬	
Sericite	▬	▬		
Ankerite	▬	▬		
Albite	▬			
Epidote	▬			
Chlorite	▬			
Tourmaline	▬			
Calcite		▬	▬	
Chalcopyrite		▬		
Native gold		▬		
Tetrahedrite		▬		
Sphalerite		▬		
Galena		▬		
Siegenite		▬		
Gersdorffite		▬		
Cobaltine		▬		
Siderite		▬		
Molybdenite		▬		
Goethite				▬
Limonite				▬
Dickite				▬

Note: Width of lines corresponds to the relative abundance of minerals of each stage.

Center for Geoanalysis, Chinese Academy of Geological Science, Beijing, China.

Carbon and oxygen isotope analysis of calcite were carried out using a Multiflow-ISOPRIME by the method of McCrea (1950) at The State Key Laboratory of Geological Processes and Mineral Resources, China University of Geosciences, Beijing, China.

5. Results and discussions

5.1. Pyroelectric property of pyrite and estimation for temperature of formation

Pyroelectric properties of pyrite can be used to study temperature of formation. Pyrite is considered as a semiconductor (Gomes et al., 2003) and its pyroelectric coefficient (α) can be calculated by the equation $\alpha = E/\Delta t$ (Li et al., 1996a). The charge carrier has positive sign in P-type pyrite and negative sign in n-type pyrite, and according to it, the conductivity of pyrite is divided into two types: negative-type (N-type, $\alpha < 0$ μV · °C^{-1}) and positive-type (P-type, $\alpha > 0$ μV · °C^{-1}) (Shao et al., 1990).

The analysis of pyroelectric properties is most accurate if pyrite is 250–400 μm in size (Shao et al., 1990; Li et al., 1996a; Chen et al., 2010). In the Huachanggou gold deposit, stage I pyrite is mostly >2 mm in size. Stage II pyrite is mostly <0.5 mm, and gold exists mainly in stage II veins. Thus, only stage II pyrite could be analyzed in the study, and the acquired data are listed in Table 3.

Stage II pyrite exhibits a frequency of 16.67–90.00% for P-type pyrite in ore zone I. Almost all the pyrite samples from ore zones II and III are N-type. Temperature of formation of the pyrite was calculated using equations: $t = (704.51 + \alpha)/1.818$ for N-type and $t = 3(122.22 + \alpha)/5.0$ for P-type (Hollister, 1985; Chen et al., 2010). The temperatures of formation of stage II pyrite from ore zones I, II and III are 144.6–306.4 °C, 168.4–339.3 °C and 199.0–312.8 °C, with pronounced modes at 220–280 °C, 240–300 °C and 240–300 °C, respectively (Fig. 8).

5.2. Ore-forming elements

The trace element composition of ores of the Huachanggou gold deposit is listed in Table 3. Ore zones II and III have a similar trace element composition of ores, but they are different when compared to ore zone I. Commonly, the enrichment factor (EF) developed by Chester and Stoner (1973) and recommended by IAEA is applied to evaluate the enrichment of elements, and it is calculated by the following equation:

$$EF = (X/M)_{sample}/(X/M)_{rock},$$

where $(X/M)_{sample}$ is the ratio of the concentration of X to a reference element M in samples; $(X/M)_{rock}$ is the ratio of the same elements in wall rocks. The reference element is the key for the evaluation (Peng et al., 2011). Previous studies have argued that Sc, Co, Cr, Cs, Th, Zr, Hf, Nb and Ta are frequently selected to be the reference element for EF calculation, owing to their not submitting to geochemical processes (Nesbitt and Markovics, 1997; Das et al., 2008; Bur et al., 2009). In this study, the concentration of Co varies relatively in minor variation (coefficient variation, CV = 0.35; Table 3), and Co is selected as a reference element for EF calculation.

Liu et al. (2012), Liu et al. (2013a) studied the trace element composition of the wall rocks from the Huachanggou gold deposit and gave out the average content values of trace elements. Both the wall rocks in ore zones II and III are phyllite and limestone from the Sanhekou Group and they shear the same average trace element composition. Spilite is the host of ore zone I, and thus, ore zone I exhibits a different average composition. The EF values of most elements have a smaller median value but a bigger arithmetic mean value. The median is the value of the middle one in a set of values when they are arranged in order; if significant variation occurs in the values, especially a few values are striking higher or lower than the rest ones, the median will be fairer to evaluate the intermediate level of the values (Bovik et al., 1983; Rousseeuwa and Crouxa, 1993). Here we use EF = 1.0 as an assessment criterion to identify the enrichment or depletion of trace elements. EF ≥ 2 indicates significant enrichment, and EF ≤ 2 indicates significant depletion.

Then the EF values are calculated and illustrated in Fig. 9, with the average composition of wall rocks. The enrichment degrees of different elements vary from each other and from different ore zones. Au is extremely highly enriched in the three ore zones (median EF = 352.44, 94.35 and 63.65 for ore zones I, II and III, respectively; Figs. 9a, c, e). Ag is moderately enriched in ore zone I (median EF = 1.81; Fig. 9a), and highly enriched in ore zone II (median EF = 6.09; Fig. 9c) and ore zone III (median EF = 4.51; Fig. 9e). As is highly enriched in the three ore zones (median EF = 5.12, 2.62 and 7.41 for ore zones I, II and III, respectively; Figs. 9a, c, e). Cu is moderately depleted in ore zone I (median EF = 0.57; Fig. 9a) but moderately enriched in ore zone II (median EF = 1.70; Fig. 9c) and ore zone III (median EF = 1.49; Fig. 9e). Mn, Mo and Ni are highly depleted in ore zones II and III (median EF < 0.5; Figs. 9e, f), and moderately depleted in ore zone I (Fig. 9a). Other elements including Bi, Cd, Hg, Pb, Sb, W and Zn exhibit small variations in the EF values, and they are slightly–moderately enriched or depleted in the ore zones.

Hierarchical cluster analysis (HCA) is an effective graphical statistical method which separates geochemical data into a hierarchy of clusters or groups on the basis of similarities (Rose et al., 1979; Reed et al., 1997; Lin et al., 2014). Generally, the method analyzing the correlations between variables is termed R-mode (Johnson and Wichern, 1988). In this study, the variable is elemental concentration, and R-mode hierarchical cluster analysis (R-HCA) is used to evaluate the relationship between Au and other elements. After standardizing and scaling the data to values between 0 and 1, Euclidean distance was used for cluster statistics, and then a dendrogram was created using the Ward method (Zhang et al., 2010). The results are presented in Figs. 9b, d, f.

The X-axis (linkage distance) represents the grade of correlation. Correlation will weaken with the decrease of linkage distance and vice versa. In the three dendrograms, the elements can all be classified into two main groups using the linkage distance of 20 as a cut off value. A

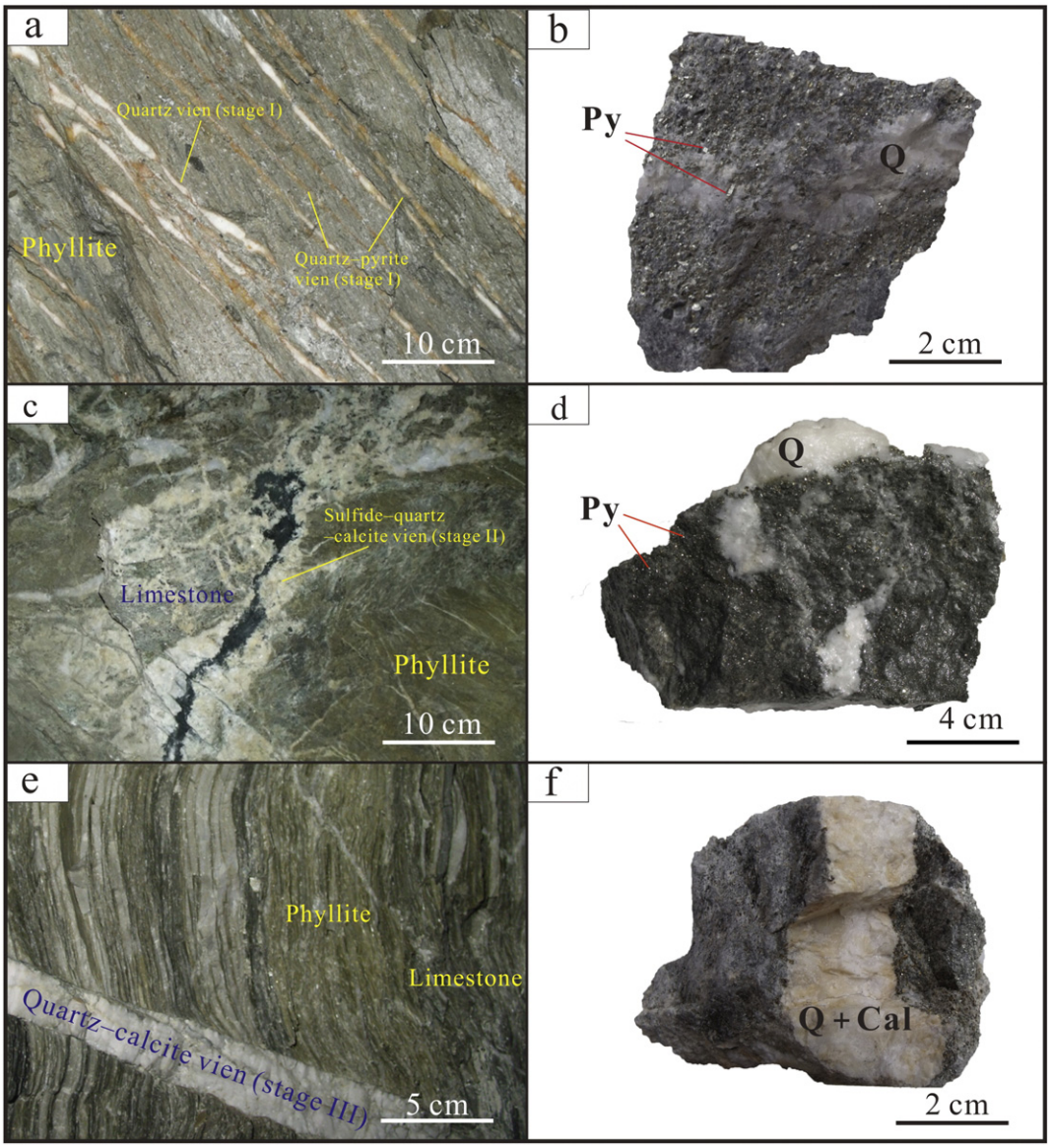

Fig. 6. Photographs showing the features of mineralization stages of the Huachanggou gold deposit. a. Stage I quartz veins occur along the stratigraphic bedding planes. b. Stage I idiomorphic cubic pyrite crystals disseminated within quartz vien. c. Stage II quartz–polymetallic sulfide veins filled along the fractures. d. Stage II hypidiomorphic–allotriomorphic pyrite crystals as dissemination. e. Stage III quartz–carbonate vein cut the strata and the early formed quartz veins. f. Stage III quartz–calcite vein without pyrite. Py = pyrite; Q = quartz; Cal = calcite.

high-grade correlation between the elements is evaluated on the basis of clustering in one dendrogram below the cut off value of linkage distance = 5. In ore zone I, Au and Ag are strongly correlated together (Fig. 9b). In ore zone II, Au, Ag and Cu are strongly correlated together (Fig. 9d). In ore zone III, Au and Ag are strongly correlated together (Fig. 9f).

In the western Qinling region, the Carlin-type gold deposits, which include the La'erma and Jinlongshan gold deposits, have an ore-forming element assemblage of Au–As–Sb–Hg–Ba–(Se) (Liu et al., 2015a). The Carlin-like gold deposits show different element assemblages, e.g., Au–Sb–Bi for the Shuangwang gold deposit (Li et al., 2000) and Au–As–Pb–Zn–Bi–Ti for the Liba gold deposit (Zhang and Wang, 2013). In the Huachanggou gold deposit, As is highly enriched in the three ore zones. However, As and Au are clustered into the same main group but different subgroup in ore zone I (Fig. 9b), and they are clustered into different main groups in ore zones II and III (Figs. 9d, f), indicating that As exhibits a weak correlation with Au. Thus the ores show a simple element assemblage of Au–Ag, which is an obvious difference between the Huachanggou orogenic gold deposit and other types of gold deposits.

5.3. Fluid inclusion characteristics and implications for the composition of ore-forming fluids

5.3.1. Fluid inclusion data

Fluid inclusions are abundant in the quartz formed during mineralization stages I to III. Two major types of fluid inclusions are distinguished (Fig. 10), viz., aqueous-solution two-phase inclusions (type I) and CO_2-rich three-phase inclusions (type II). Type I fluid inclusions are composed of vapor and liquid water, of which vapor accounts for 5 to 30% of the total volume. They exhibit oval, trilateral and irregular shapes and generally vary from 4 to 10 μm in size (occasionally to 20 μm). Type II fluid inclusions are composed of liquid CO_2, gaseous CO_2 and liquid H_2O, of which CO_2 accounts for 5 to 20% of the total inclusion volume. They are generally 5–15 μm in size and elliptical in shape. Commonly, the type II fluid inclusions are present as isolated inclusions,

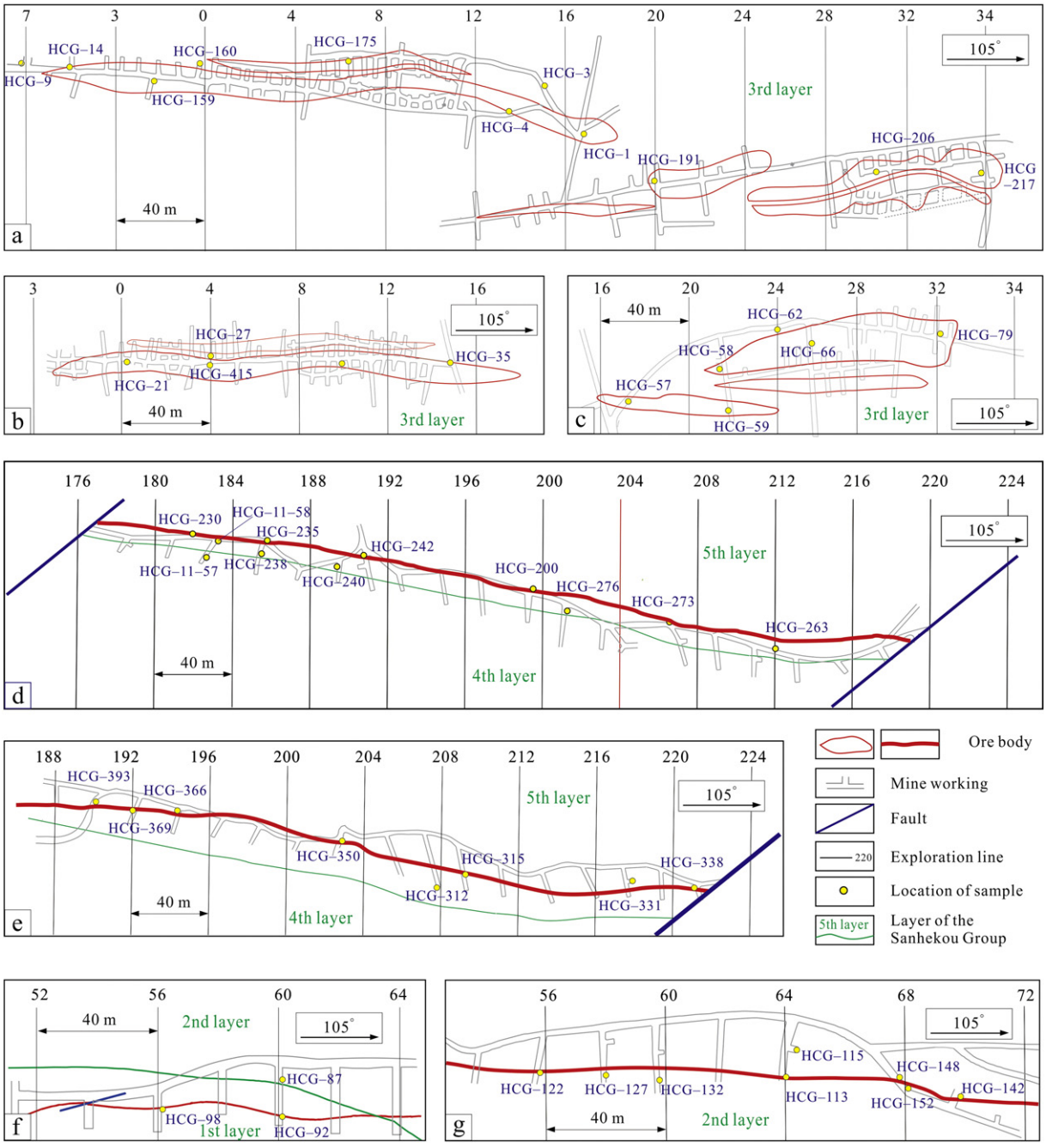

Fig. 7. Maps of different levels of the Huachanggou gold deposit, showing locations of samples collected from the different mining workings. a. Ore zone I; level 1150 m. b. Ore zone I; level 1100 m. c. Ore zone I; level 1070 m. d. Ore zone II; level 950 m. e. Ore zone II; level 910 m. f. Ore zone III; level 1030 m. g. Ore zone III; level 990 m.

occur along growth planes, as clusters, or coexist with type I fluid inclusions (Fig. 10c, e). In addition, a small number of carbonic fluid inclusions (type III), which are composed of gaseous or/and liquid CO_2, are also distinguished. They are 3–8 μm in size and exhibit rounded and elliptical shapes (Fig. 10c, e).

5.3.2. Physical and chemical conditions of mineralization

The authors systematically measured temperature of homogenization and calculated the salinity of the fluid inclusions hosted in quartz. Microthermometric results are listed in Table 4 and illustrated in Fig. 11. In ore zone I, the temperatures exhibit pronounced modes at 300–340 °C, 240–300 °C and 200–240 °C for stages I, II and III, respectively (Fig. 11a). Estimated salinities are 0.9–12.0 wt.% NaCl equiv. for type I inclusions and 1.0–9.8 wt.% NaCl equiv. for type II inclusions. In ore zone II, the temperatures exhibit pronounced modes at 280–320 °C, 200–260 °C and 140–220 °C for stages I, II and III, respectively (Fig. 11b). Estimated salinities are 0.5–9.8 wt.% NaCl equiv. for type I inclusions and 1.0–4.7 wt.% NaCl equiv. for type II inclusions. In ore zone III, temperatures exhibit pronounced modes at 300–340 °C, 220–280 °C and 160–240 °C for stages I, II and III, respectively (Fig. 11c). Estimated salinities are 0.9–10.7 wt.% NaCl equiv. for type I inclusions and 2.6–5.2 wt.% NaCl equiv. for type II inclusions.

Vapor and liquid phase composition data of fluid inclusions are listed in Table 5. The cations in ore-forming fluids are principally Ca^{2+}, with secondary Na^{+}, K^{+} and Mg^{2+}. The anions are mostly SO_4^{2-} and Cl^{-}, with a minor content of NO_3^{2-} and F^{-}. Note that the SO_4^{2-} content in this study cannot represent the original composition of fluid in the fluid inclusions, because the other possible S-bearing species

Table 3
Pyroelectric coefficient of stage II pyrite and trace element composition of ores from the Huachanggou gold deposit.

Sample no.	Pyroelectric coefficients of pyrite (μV · °C^{-1})				Trace element compositions of the ores (ppm)														
	N-type		P-type		Au	Ag	As	Bi	Cd	Co	Cu	Hg	Mn	Mo	Ni	Pb	Sb	W	Zn
	Range	α	Range	α	(ppb)	(ppb)		(ppb)	(ppb)			(ppb)							
Ore zone I																			
HCG-1	−258 to −46	−187.5	47 to 268	122.5	6548	33	44.72	47	185	23.9	9.5	9.3	2790	1.58	43.2	4.7	0.28	10.35	104.2
HCG-159	−262 to −50	−198.7	51 to 222	136.5	1231	31	421.04	157	93	52.5	11.4	11.1	1308	0.17	69.9	5.6	1.82	14.79	54.2
HCG-206	−262 to −52	−157.9	44 to 414	118.8	4417	121	145.72	217	70	66.4	7.8	8.8	1751	0.2	76.9	6.2	1.31	17.04	67.7
HCG-217	−258 to −79	−173.5	69 to 309	178.1	4794	36	90.44	89	82	33	67.5	6.4	1455	0.27	66.4	4.4	1.58	18.87	53.4
HCG-21	−251 to −222	−243.2	76 to 625	289.4	10,570	220	17.76	52	35	5.6	15.5	1.2	436	0.16	9.2	1.7	0.37	5.6	17.1
HCG-415	−272 to −52	−200.6	66 to 321	177.1	1443	73	90.70	144	92	45.2	99.5	21.9	1347	0.12	56.8	4.7	1.61	16.9	81.2
HCG-59	−216 to −44	−147.5	61 to 279	131.8	2525	77	78.10	114	74	46.8	44.5	5.8	1481	0.19	83.7	6.3	1.24	11.38	62.2
HCG-79-2	−140 to −56	−87.8	73 to 519	204.7	9412	74	28.50	100	78	42.6	19.7	7.0	1137	0.38	53.6	2.4	1.43	28.58	61.8
Ore zone II																			
HCG-230	−272 to −56	−215.9	56 to 277	158.5	1711	94	66.40	493	100	12.7	24.9	14.0	1554	0.12	9.3	22.8	0.35	2.88	68.4
HCG-235	−267 to −89	−226.5	47 to 523	254.4	14,110	1100	222.81	1538	94	34.6	40.8	28.6	1297	0.19	17.7	38.5	1.17	5.47	72.1
HCG-242	−268 to −67	−241.8	ND	ND	2312	105	34.35	102	61	6.8	6.2	10.5	693	0.14	15.2	9.1	0.5	3.18	52. 9
HCG-273	−272 to −49	−215.6	ND	ND	4011	237	88.48	854	121	13.6	30.3	20.4	1615	0.38	8.4	22.1	0.89	10.3	54.3
HCG-278	−268 to −46	−191.6	51 to 202	98.3	4993	308	108.70	1412	117	36.4	37.4	36.8	1681	0.26	14.7	57.7	2.43	7.79	146.8
HCG-315	−276 to −80	−225.8	ND	ND	31,503	1789	44.59	2338	203	61.4	240.1	62.5	1006	0.15	19.3	90.8	3.53	3.84	160.6
HCG-338	−268 to −79	−226.7	ND	ND	22,203	761	347.98	1132	136	37.6	33.9	96.6	1026	0.29	27.1	40.6	0.8	4.1	130.4
HCG-369	−275 to −111	−245.7	ND	ND	3821	155	49.83	56	46	21.1	27.9	11.5	315	0.1	26.3	5.6	1.09	7.02	192.2
Ore zone III																			
HCG-98	−273 to −66	−204.5	132 to 286	209.4	9302	467	490.88	433	109	34.5	84.5	135.4	1152	0.1	14.5	16.4	5.77	9.95	89.7
HCG-92	−270 to −123	−245.5	ND	ND	5517	154	370.04	699	113	40.5	35	18.1	774	0.2	19.2	28.6	0.83	10.62	136.6
HCG-113	−270 to −58	−232.6	ND	ND	27,928	1441	851.85	1080	102	45.1	57.6	48.4	983	0.53	24.7	22.6	1.75	11.19	102.3
HCG-122	−272 to −86	−164.3	ND	ND	5950	404	879.04	967	142	37.4	90.2	14.0	1472	0.2	17.6	41	1.03	6.51	52
HCG-142	−286 to −86	−187.3	ND	ND	30,770	538	353.93	770	62	23.9	22.1	25.1	971	0.53	15.2	22.9	1.32	6.87	86.9
HCG-152	−226 to −83	−207.7	ND	ND	4810	406	357.18	2232	53	42.6	16.1	59.5	966	0.71	17.6	39.6	2.24	5.86	60.8

(e.g., H_2S, HS^- and HSO_4^-) in the fluid inclusions had been oxidized to SO_4^{2-} during the thermal decrepitation process in the test. The vapor phase is chiefly composed of H_2O, CO_2 and N_2, with a minor content of CH_4, C_2H_2 and C_2H_4. Thus the ore-forming fluid can be represented by a "salt solution–CO_2" hydrothermal system.

The ore-forming fluids in the Huachanggou gold deposit were of medium temperature (135–365 °C) and moderate-low salinity (0.9–12.0 wt.% NaCl equiv.). The petrography of the fluid inclusions reveals the coexistence of different types of fluids. Different types of fluid inclusions display similar homogenization temperatures. Many fluid inclusions formed at the same stage have a similar temperature of homogenization but quite different salinities. These data strongly indicate a role for boiling of the fluid during the mineralization process.

5.4. Stable isotope geochemistry

5.4.1. Sulfur isotope data

The average $\delta^{34}S$ ratio of sulfide minerals can be used to characterize the source of sulfur under conditions where H_2S is the dominant sulfur species in the fluid (Ohmoto and Rye, 1979; Rollinson, 1993). In the Huachanggou gold deposit, the sulfur-bearing minerals are sulfides linked to the main mineralization stage, and pyrite is the most abundant sulfide mineral. Sulfur isotope ratio data are listed in Table 6. Stage II pyrite exhibits relatively low $\delta^{34}S$ ratio which ranges from −8.3 to 1.0‰ with a pronounced range of −4 to 1‰. Significant differences occur among different ore zones. These $\delta^{34}S$ ratios are distributed in a relative narrow range of −3.1 to 1.0‰ for ore zone I and vary between −8.0 and −0.6‰ for ore zone II and between −8.3 and 0.8‰ for ore zone III.

The $\delta^{34}S$ ratios of ore zones II and III have relatively broad ranges with a variation of 9.1‰ (from −8.3 to 0.8‰), indicating that sulfur isotope ratio of pyrite had not reached equilibrium, which is consistent with the phenomenon of boiling (Liu et al., 2015a,b). The $\delta^{34}S$ ratio range of pyrite hosted in spilite is much narrower than that of pyrite hosted in limestone, but their median values are quite similar (−0.9‰ for the former and −0.7‰ for the latter). These $\delta^{34}S$ ratios are also respectively corresponding to the $\delta^{34}S$ ratios of spilite (−1.3 to 4.7‰; Zhou et al., 2011b) and limestone (−26.2 to 16.4‰; Zhou et al., 2011b) from the Sanhekou Group, indicating a potential source for the sulfur from the wall rocks.

Previous studies have argued that the gold is transported as a soluble bisulfide complex along with sulfur in fluids, and the sulfidation

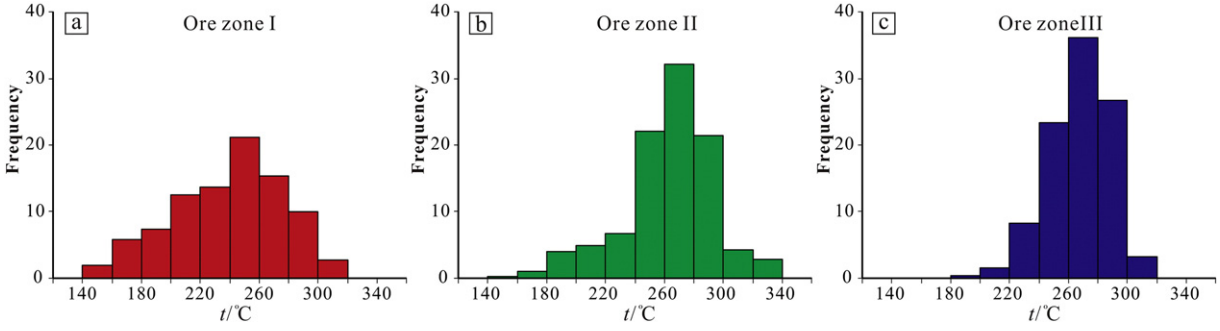

Fig. 8. Temperatures of formation of pyrite from ore zones I (a), II (b), and III (c) in the Huachanggou gold deposit.

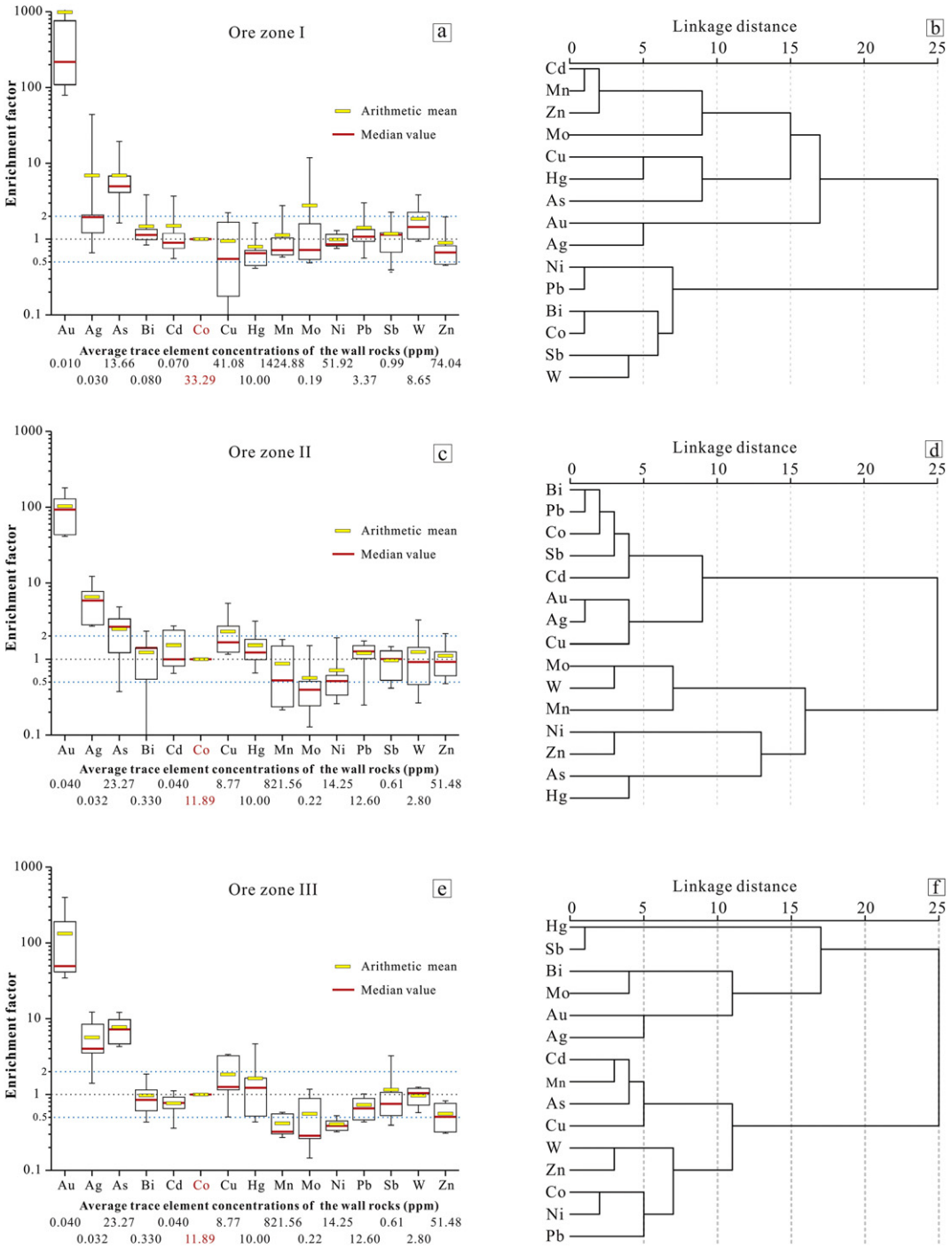

Fig. 9. Box plots showing ranges of enrichment factors (EF) of the trace element concentrations of ores for ore zones I (a), II (c), and III (e), with the average concentration data from Liu et al. (2012), Liu et al. (2013a); R-mode hierarchical cluster analysis dendrograms of the trace element concentrations of ores for ore zones I (b), II (d), and III (f).

of iron-bearing minerals in the host rocks is the cause of pyritization and gold deposition in orogenic gold deposits (Hofstra and Cline, 2000; Kesler et al., 2003; Goldfarb et al., 2005; Large et al., 2011). Abiotic thermochemical reduction of sulfate can cause a fractionation of 10–25‰ in the $\delta^{34}S$ ratio of sulfide (Harrison and Thode, 1957; Seal, 2006). The sulfide $\delta^{34}S$ values in most sediment-hosted gold deposits have a mode consistently 15–20‰ lighter than coeval seawater sulfates, owing to the reduction of seawater sulfate in sedimentary wall rocks (Chang et al., 2008; Large et al., 2011). The $\delta^{34}S$ value of modern seawater is very stable around 21‰ (Rees et al., 1978; Hoefs, 1997); however, the value frequently fluctuated through geologic time (Claypool et al., 1980; Chen and Chu, 1988; Holser et al., 1996). The Sanhekou Group, which hosts the Huachanggou gold deposit, was formed during Middle–late Devonian (Du et al., 1998; Dong, 2004). The $\delta^{34}S$ value of seawater sulfates in Middle–Lower Devonian marine evaporite ranges from 15.6 to 21.8‰, with an average of 18.24‰ and a median of 18.5‰ (Claypool et al., 1980, and references therein). The $\delta^{34}S$ values of hydrothermal pyrite in the deposit range from −8.3 to 0.8‰, with an average of −1.85‰ and a median of −0.7‰. These data are about 20‰ lighter than the coeval seawater sulfates. In addition, spilite was formed by marine volcanic exhalative sedimentation, thus sea water played a role in the homogenization of sulfur in spilite. We propose that seawater sulfate was the source of the sulfur in the deposit.

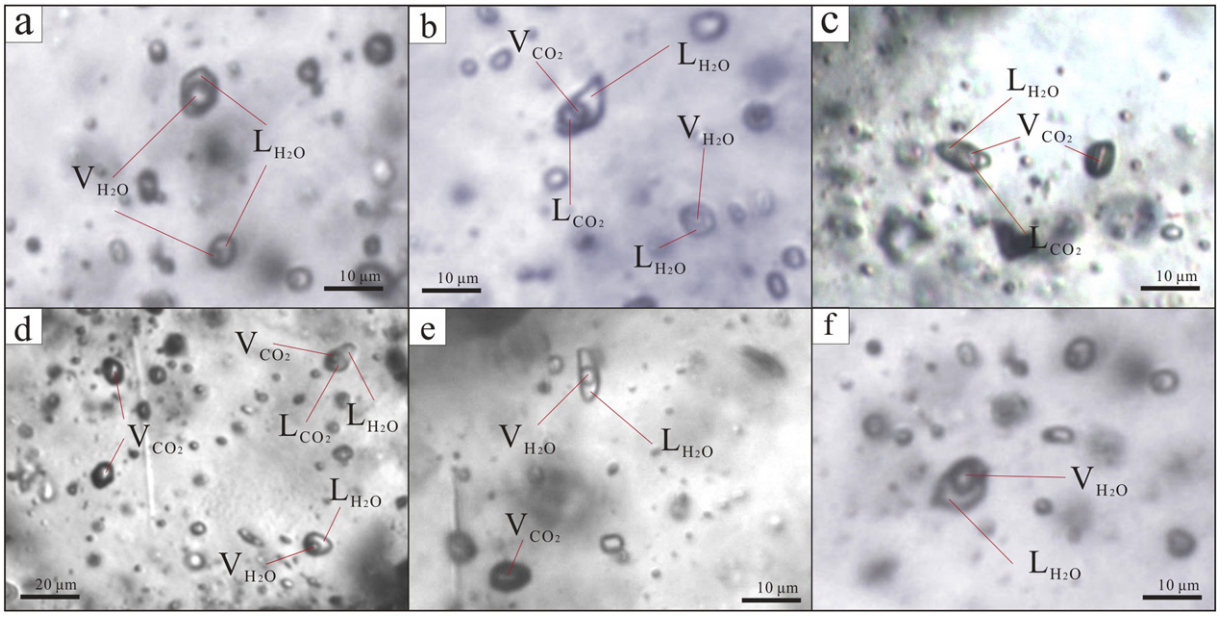

Fig. 10. Microphotographs of representative fluid inclusions in quartz from the Huachanggou gold deposit. a. Type I fluid inclusions in stage I quartz. b. Coexisting type I and type II fluid inclusions in stage II quarzt. c. Coexisting type II and type III fluid inclusions in stage II quartz. d. Coexisting type I and type II fluid inclusions in stage II quartz. e. Coexisting type I and type III fluid inclusions in stage II quarzt. f. Type I fluid inclusion in stage III quartz.

5.4.2. Lead isotope

The lead isotope ratios in Pb-bearing mineral depend on the initial concentration of U and Th and the time since the mineral was formed (Gulson, 1986; Shen, 1987). Pb-bearing minerals hold very low U/Pb and Th/Pb ratios compared to ordinary rocks, and their Pb isotopic composition remaineds constant since their formation (Viets and Leach, 1990; Harlavan et al., 1998; Hansmann and Koppel, 2000). Lead isotope ratios have contributed significant constraints to the understanding of the genesis of lead in gold deposits (e.g., Chernyshev et al., 2011; Chugaev et al., 2014; Standisha et al., 2014; Zhang et al., 2014; Jiang et al., 2015).

Lead isotope ratios of pyrite from the Huachanggou gold deposit are listed in Table 6 and illustrated in Fig. 12. Ore zone I has a limited variation in the ratios and a uniform Pb isotopic composition. The Pb isotope ratios of ore zones II and III are similar. Notwithstanding, these Pb isotope ratios of the three ore zones exhibit a good linear relationship, with high correlation coefficients ($R = 0.982$ for $^{207}Pb/^{204}Pb$ vs $^{206}Pb/^{204}Pb$, and $R = 0.948$ for $^{208}Pb/^{204}Pb$ vs. $^{206}Pb/^{204}Pb$) (Fig. 12). Thus the ores from different ore zones may have a similar Pb isotope evolution.

To characterize the tectonic setting of source region of the lead in the ores, the data from various ore zones have been plotted against the different evolutionary curves of Pb tectonic models (Fig. 12). In Fig. 12a, the data for ore zone I plot between the mantle and the orogenic Pb evolutionary curve, indicating a lower crust or mantle source for the lead. The data for ore zones II and III plot between the upper crust and the orogenic Pb evolutionary curves, indicating an upper crustal source for the lead. In Fig. 12b, all of the data plot between the lower crust and the orogenic Pb evolutionary curves, indicating the lower crustal source for the lead.

Table 4
Microthermometric data of fluid inclusions in quartz from the Huachanggou gold deposit.

Mineralization stage	FI type	Num.	Tm(ice) (°C)	Tm(cla) (°C)	Th(CO_2) (°C)	Th(tot) (°C)	Salinity (wt.% NaCl eq.)
Ore zone I							
I	I	16	−6.7 to −2.3			271–361	3.9–10.1
II	I	50	−8.3 to −0.5			200–365	0.9–12.0
II	II	10		4.5–9.5	23.4–27.5	230–328	1.0–9.8
III	I	53	−6.4 to −2.3			162–264	3.9–9.8
III	II	8		4.7–8.3	15.7–28.5	183–283	3.6–9.6
Ore zone II							
I	I	12	−5.5 to −1.5			260–365	2.6–8.5
II	I	67	−6.2 to −0.5			150–321	0.5–9.5
II	II	8		7.6–9.5	23.0–27.2	272–295	1.0–4.7
III	I	54	−6.4 to −0.9			135–287	1.6–9.8
Ore zone III							
I	I	9	−5.7 to −4.2			264–349	6.8–8.8
I	II	5		7.6–8.4	13.8–22.7	250–345	3.2–4.7
II	I	35	−7.1 to −0.5			175–313	0.9–10.7
II	II	5		7.3–8.7	25.0–25.5	251–265	2.6–5.2
III	I	27	−5.1 to −2.1			147–298	3.5–8.0
III	II	2		7.9–8.0	20.7–21.0	219–220	3.9–4.1

Tm(CO_2), initial melting temperature of CO_2; Tm(ice), freezing temperature; Tm(cla), clathrate melting temperature; Th(CO_2), homogenization temperature of CO_2; Th(tot), total homogenization temperature. The salinities of fluid inclusions are estimated using the data from Collins (1979) and Bodnar (1993).

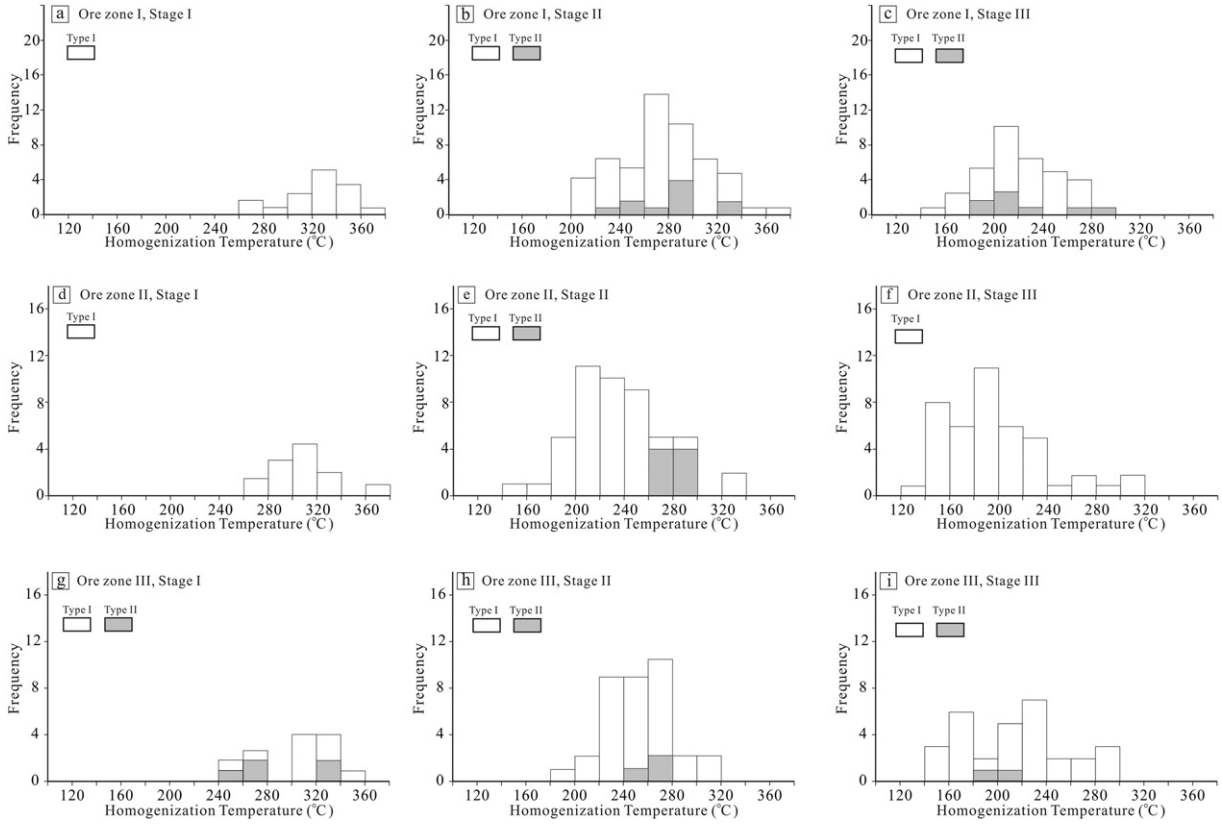

Fig. 11. Temperature of homogenization of fluid inclusions in quartz from the Huachanggou gold deposit.

A $\Delta\beta - \Delta\gamma$ diagram established by Zhu (1998) is also used in this study to help in establishing the source of lead (Fig. 13). This diagram was established based on the ranges of $\Delta\beta$ and $\Delta\gamma$ values of lead from various types of rocks and ores. $\Delta\beta$ and $\Delta\gamma$ values are calculated according to the equations $\Delta\beta = (\beta - \beta_M) \times 1000/\beta_M$ and $\Delta\gamma = (\gamma - \gamma_M) \times 1000/\gamma_M$ (β: $^{207}Pb/^{204}Pb$ of sample, β_M: $^{207}Pb/^{204}Pb$ of mantle, γ: $^{208}Pb/^{204}Pb$ of sample, γ_M: $^{208}Pb/^{204}Pb$ of mantle; Zhu, 1998). This diagram has been applied in the study of the lead source of gold deposits (e.g., Zhang et al., 2009, 2014; Yang et al., 2012b; Jiang et al., 2015). To calculate the $\Delta\gamma$ and $\Delta\beta$ values, the age of gold mineralization used here is 215 Ma which has been discussed in Section 2 (Regional geology). The $\Delta\gamma - \Delta\beta$ diagram indicates a combination of upper crust and mantle lead for ore zone I and an upper crust lead for ore zones II and III (Fig. 13). Spilite is a kind of magmatic rock which may contain the lead derived from mantle so that the mixed lead for ore zone I can be interpreted that spilite had provided lead. Thus the lead of the Huachanggou gold deposit appears to have been derived from the wall rocks.

5.4.3. Hydrogen and oxygen isotopes

Oxygen and hydrogen isotope data are an important monitor for the source and evolution of fluids (Arribas et al., 1995; Hoefs, 1997). The H and O isotopic composition of quartz from different ore zones of the

Table 5
Vapor and liquid phase composition of fluid inclusions from the Huachanggou gold deposit (ppm).

Stage	I	II		III	
Sample no.	HCG-3	HCG-416	HCG-11-57	HCG-9	HCG-58
Na^+	1.3	1.8	1.12	1.1	1.5
K^+	4.2	1.7	1.4	1.3	2.4
Mg^{2+}	1.1	1.2	1.0	1.3	1.1
Ca^{2+}	13.0	13.2	12.6	42.6	10.9
F^-	0.504	0.144	0.127	0.424	1.147
Cl^-	1.391	1.734	2.727	1.455	1.954
NO_2^-	0.042	0.078	0.162	0.152	0.069
NO_3^-	0.558	0.660	0.845	0.228	0.599
SO_4^{2-}	4.540	9.691	5.419	5.447	5.473
CH_4	0.6	0.6	0.3	0.2	0.1
$C_2H_2 + C_2H_4$	0.5	0.3	0.2	0.3	0.2
CO_2	151.0	346.4	124.4	92.3	42.9
H_2O	576.1	525.6	151.4	135.2	197.4
O_2	8.0	25.3	10.9	8.9	5.1
N_2	43.0	126.5	52.6	43.3	23.4
CO		31.0			10.1

Table 6
Sulfur and lead isotopic composition of stage II pyrite from the Huachanggou gold deposit.

Sample no.	$\delta^{34}S_{V\text{-}CDT}$‰	$^{206}Pb/^{204}Pb$	$^{207}Pb/^{204}Pb$	$^{208}Pb/^{204}Pb$
Ore zone I				
HCG-62	−0.6	17.926	15.557	38.255
HCG-66	0.3	17.905	15.549	38.215
HCG-79	−3.1	17.873	15.532	38.120
HCG-4	−1.2	17.891	15.548	38.221
HCG-14	0.4	17.835	15.545	38.282
HCG-27	1.0	17.892	15.546	38.197
HCG-160	−2.4	18.018	15.559	38.294
HCG-191	−1.8	17.875	15.535	38.158
Ore zone II				
HCG-263	−0.7	18.221	15.622	38.683
HCG-312	−0.6	18.125	15.594	38.583
HCG-366	−8.0	18.294	15.639	38.938
HCG-276	−3.0	18.332	15.624	39.270
Ore zone III				
HCG-92	−8.3	18.306	15.645	38.799
HCG-122	0.8	18.280	15.633	38.870
HCG-152	−0.5	18.340	15.647	38.848

Notes: $\delta^{34}S$ values were reported relative to the Vienna Cañon Diablo Troilite (V-CDT). An uncertainty of ±0.2‰ is recommended. Standard errors are within 0.004 for $^{206}Pb/^{204}Pb$, within 0.003 for $^{207}Pb/^{204}Pb$, and within 0.007 for $^{208}Pb/^{204}Pb$.

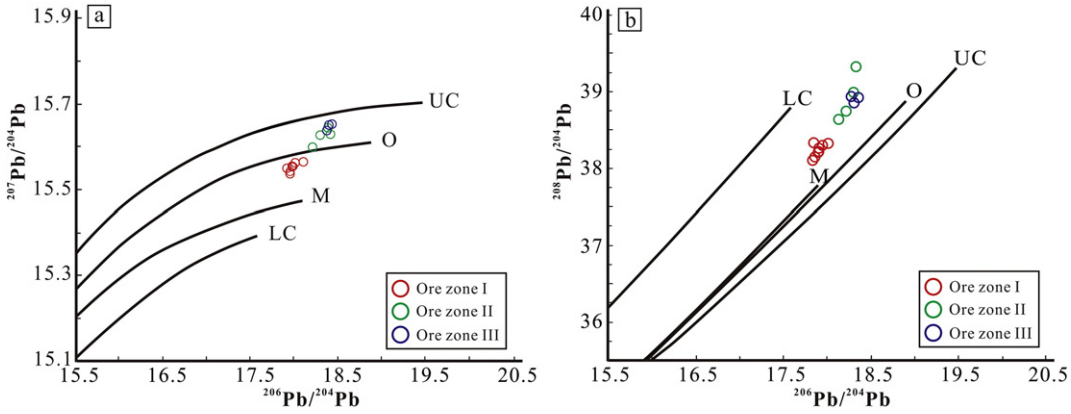

Fig. 12. Lead isotopic composition of pyrite from the Huachanggou gold deposit. The Pb tectonic model models after Zartman and Doe (1981): O = orogen; M = mantle; UC = upper crust contributed to the orogen; LC = lower crust contributed to the orogen. Dotted curves show the lead evolutions fit the data.

Huachanggou gold deposit is listed in Table 7. The $\delta^{18}O$ values of ore-forming fluids ($\delta^{18}O_W$) were calculated from the $\delta^{18}O$ values of quartz ($\delta^{18}O_Q$). δD values were obtained by measuring fluid inclusions in quartz.

In the Huachanggou gold deposit, no Indosinian magmatism is documented, which precludes a magmatic source for the ore-forming fluids. The calculated $\delta^{18}O_w$ and δD values for stage I are close to the values of metamorphic water (Li and Tai, 2007; Zhou et al., 2014; Fig. 14), and the values for stages II and III are distributed between the range of metamorphic water and meteoric water.

The oxygen and hydrogen isotopic composition of fluid is controlled by both the isotopic composition of initial fluid and wall rocks and the temperature and water/rock ratio (W/R) during water–rock interaction; it is possible to assess the evolution of water–rock isotopic exchange (Taylor, 1974):

$$W \cdot \delta^{i}_{water} + R \cdot \delta^{i}_{rock} = W \cdot \delta^{f}_{water} + R \cdot \delta^{f}_{rock},$$

where i = initial value; f = final value after exchange; W = atomic percent of fluid; R = atomic percent of exchangeable rock;

$$W/R = \left(\delta^{f}_{rock} - \delta^{i}_{rock}\right) / \left[\delta^{i}_{water} - \left(\delta^{f}_{rock} - \Delta\right)\right],$$

where $\Delta = \delta^{i}_{rock} - \delta^{f}_{water}$. W/R is the value of atomic ratio. Oxygen and hydrogen contents are normally about 50% and 1% in rocks, respectively (Liu et al., 1998; Zheng and Chen, 2000; Guo et al., 2014). The mass ratio of water to rock can be calculated using $w(W)/w(R) = 0.5 \cdot W/R$ for the calculation of $\delta^{18}O$ and $w(W)/w(R) = 0.01 \cdot W/R$ for δD.

In the Huachanggou gold deposit, the Sanhekou Group is comprised mainly of limestone, phyllite and sandstone, and spilite is the host of the orebodies of ore zone I (Fig. 2). Based on the hydrogen and oxygen isotopic compositions of limestone, clastic sedimentary rock, metamorphic rock and spilite, the $\delta^{i}_{rock}{}^{18}O$ and $\delta^{i}_{rock}D$ values brought into calculation are set at 16‰ and −60‰ for the Sanhekou Group (without spilite), and 16‰ and −60‰ for spilite, respectively (Fig. 14; Munhá and Kerrich, 1980; Xia and Xia, 1987; Fouillac and Javoy, 1988; Shen et al., 1991; Hoefs, 1997). The values for the Mesozoic meteoric water in the Qinling region were about −16‰ and −120‰ (Zhang et al., 1995). However, the initial values of metamorphic fluid in this region are difficult to establish. The maximum $\delta^{18}O$ and minimum δD values for stage I are 13.8‰ and −78‰, thus the initial $\delta^{i}_{water}{}^{18}O$ and $\delta^{i}_{water}D$ values are assumed as 15‰ and −80‰, respectively. Fig. 14 illustrates the calculated evolutional curves at 340 °C (stage I), 260 °C, (stage II), 200 °C (stage III) and 150 °C (stage III), with W/R ratio varying from 5 to 0.005.

Despite the fact that isotopic exchange occurred during water–rock reaction associated with large-scale hydrothermal alteration, the early-stage fluid should exhibit similar features to the initial fluid and

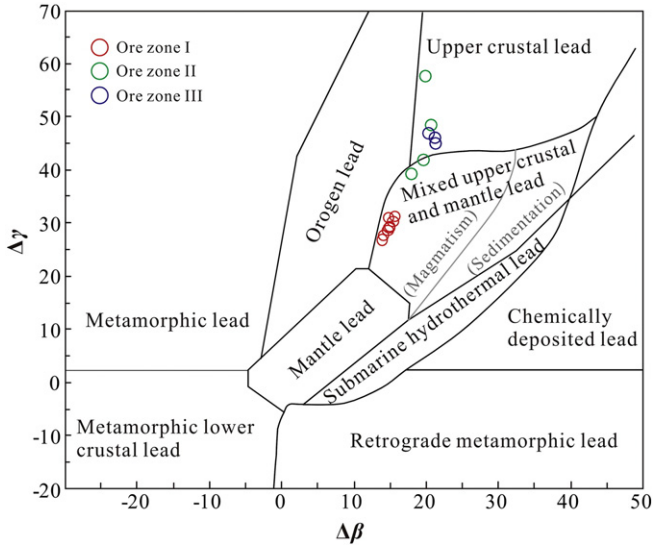

Fig. 13. Δγ–Δβ diagram of ore lead of the Huachanggou gold deposit (after Zhu, 1998).

Table 7
Oxygen and hydrogen isotopic composition of quartz and fluid inclusions from the Huachanggou gold deposit.

Sample no.	Stage	δD (‰)	$\delta^{18}O_Q$ (‰)	$\delta^{18}O_W$‰	T (°C)	Reference
Ore zone I						
TS08	I	−78	18.6	13.3	350	Li and Tai, 2007
TS09	I	−77	18.5	12.6	320	Li and Tai, 2007
HCG-175	II	−79	17.3	8.8	260	
HCG-307	II	−86	18.1	9.6	260	
HCG-58	III	−80	17.6	5.9	200	
1150-9-1	III	−71	16.8	1.3	150	Zhou et al., 2014
Ore zone II						
910-224-1	I	−68	18.0	12.4	340	Zhou et al., 2014
HCG-11-57	II	−81	17.9	9.4	260	
HCG-11-58	III	−91	20.4	5.2	180	
910-220-3	III	−70	18.2	2.3	145	Zhou et al., 2014
Ore zone III						
1030-76-1	I	−66	20	13.79	320	Zhou et al., 2014
1030-76-3	I	−67	19.1	12.89	320	Zhou et al., 2014
HCG-115	III	−102	18.5	6.8	200	
HCG-132	III	−112	20.1	8.4	200	
1030-76-4	III	−71	17.7	2.2	150	Zhou et al., 2014

Notes: $\delta^{18}O$ values of ore-forming fluids ($\delta^{18}O_W$) were calculated according to quartz–water equilibrium temperature equation $1000\ln\alpha_{Q\text{-}W} = 3.38 \times 10^6\ T^{-2} - 3.40$ (Clayton et al., 1972). δD values were obtained by analyzing fluid inclusions in quartz. Total uncertainties were estimated to be better than 0.2‰ for $\delta^{18}O$ and 0.3‰ for δD.

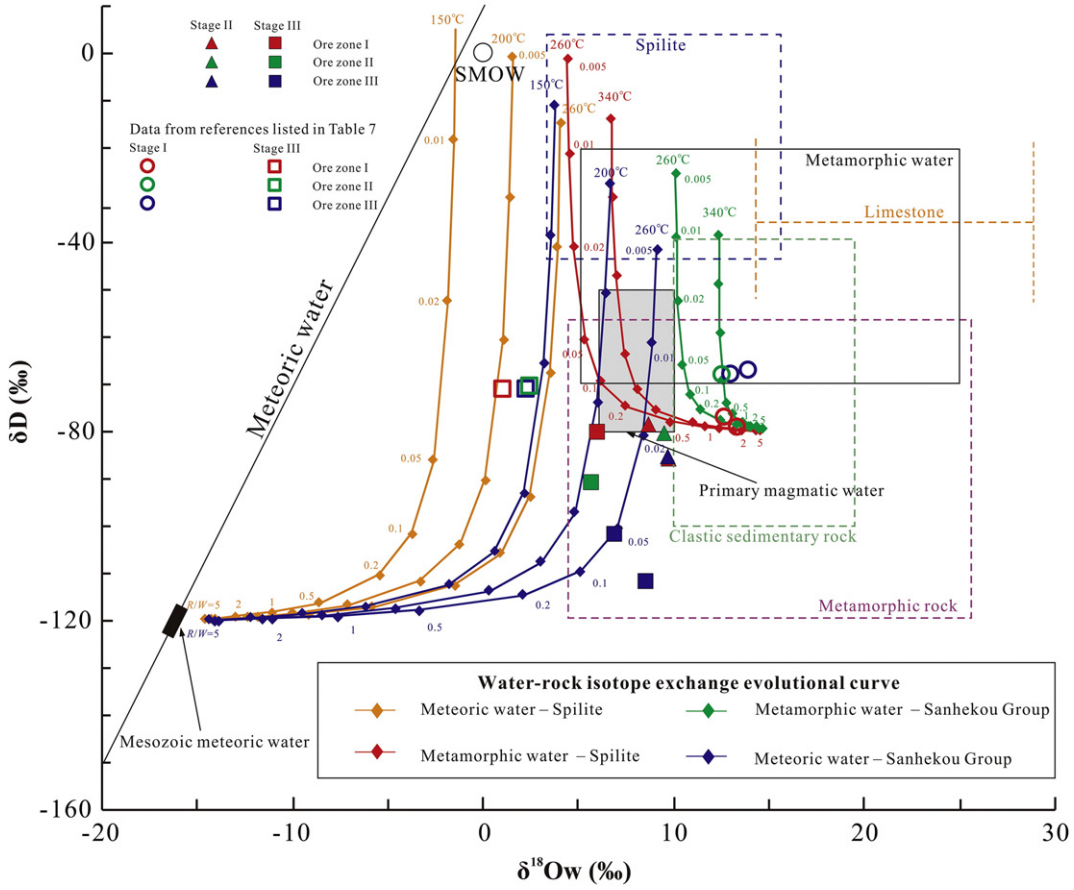

Fig. 14. Hydrogen and oxygen isotopic composition and water–rock isotope exchange evolutional curves of the Huachanggou gold deposit. Data for primary magmatic water, metamorphic water and meteoric water are from Taylor (1974); data for spilite are from Munhá and Kerrich (1980), Xia and Xia (1987), Fouillac and Javoy (1988), Shen et al. (1991); data for limestone, clastic sedimentary rock and metamorphic rock are from Hoefs (1997); data for the Mesozoic meteoric water are from Zhang et al. (1995).

can be used to constrain the original source composition (Guo et al., 2014). The values for stage I are distributed close to the metamorphic water–Sanhekou Group curve and the metamorphic water–spilite curve at 340 °C. This indicates that the initial $\delta^{18}O$ value of 15‰ is appropriate. This $\delta^{18}O$ value is in the range for normal metamorphic water (Taylor, 1974; Hoefs, 1997; Zheng and Chen, 2000). However, the δD value is lower than normal metamorphic water, and this may be the result of the mixing with meteoric water.

The values for stages II and III have a trend of migrating to the curves of water–rock exchange between meteoric water and wall rocks (Fig. 14). Because δD value increases with the decrease of W/R value (from 5 to 0.005), the δD value will be higher than the initial δD value of fluid during water–rock interaction. Therefore, the lower minimum δD values than metamorphic water also indicate mixing with meteoric water. Compared with stage II, the values for stage III are closer to the evolution curve of the Mesozoic meteoric water (Fig. 14). The meteoric water contributed more to the formation of stage III fluid.

5.4.4. Carbon and oxygen isotopes

The carbon and oxygen isotopic composition of calcite is listed in Table 8. The $\delta^{13}C_{PDB}$ and $\delta^{18}O_{SMOW}$ values range from −3.76 to −1.60‰ (average on −2.35‰) and from 15.79 to 16.80‰ (average on 16.40‰) for stage II, and from −2.20 to −0.24‰ (average −1.10‰) and from 16.47 to 19.69‰ (average 17.44‰) for stage III, respectively. In each ore zone, the $\delta^{13}C_{PDB}$ values of stage II are lower than those of stage III.

CO_2 is the dominant C-bearing species in hydrothermal fluid (Ohmoto, 1972). The $\delta^{13}C_{PDB}$ values of calcite were directly measured from CO_2 which was released during the reaction of calcite with phosphoric acid. The average $\delta^{13}C_{PDB}$ and $\delta^{18}O_{SMOW}$ values of the fluids are −2.35‰ and 16.40‰ for stage II, and −1.10‰ and 17.44‰ for stage III, respectively. These values are different from the value ranges of crustal source, atmospheric source, freshwater and organic matter (Hoefs, 1997; Schildlowski, 1998), but they are close to the values of marine limestone ($\delta^{13}C_{PDB} = 0 \pm 4‰$, $\delta^{18}O_{SMOW} = 20 - 40‰$; Liu et al., 2004, 2010). Three principal CO_2 sources are indicated (termed organic matter, marine carbonate rock and magma–mantle source). The variation trends of C and O isotopic composition during important

Table 8
Carbon and oxygen isotopic composition of calcite from the Huachanggou gold deposit.

Sample no.	Stage	$\delta^{13}C_{PDB}$ (‰)	$\delta^{18}O_{PDB}$ (‰)	$\delta^{18}O_{SMOW}$ (‰)
Ore zone I				
HCG-57	II	−1.49	−13.96	16.47
HCG-35	III	−1.68	−13.98	16.45
Ore zone II				
HCG-240	II	−2.76	−14.39	16.02
HCG-331	III	−1.60	−13.84	16.59
HCG-350	III	−1.52	−13.95	16.48
HCG-238	III	−1.18	−13.76	16.67
HCG-393	III	−0.37	−12.77	17.69
Ore zone III				
HCG-459	II	−2.64	−14.01	16.42
HCG-132	II	−2.42	−13.64	16.80
HCG-127	III	−2.39	−13.81	16.63
HCG-148	III	−2.20	−13.78	16.66
HCG-87	III	−0.24	−10.84	19.69

Notes: The data were reported in per mil relative to the Peedee Belemnite limestone (PDB) standard with total uncertainties were estimated to be better than 0.2‰ for $\delta^{18}O$ and 0.15‰ for $\delta^{13}C$. The equation ($\delta^{18}O_{SMOW} = 1.03086\delta^{18}O_{PDB} + 30.86$) by Friedman and O'Neil (1977) was used to convert $\delta^{18}O_{PDB}$ to $\delta^{18}O_{SMOW}$.

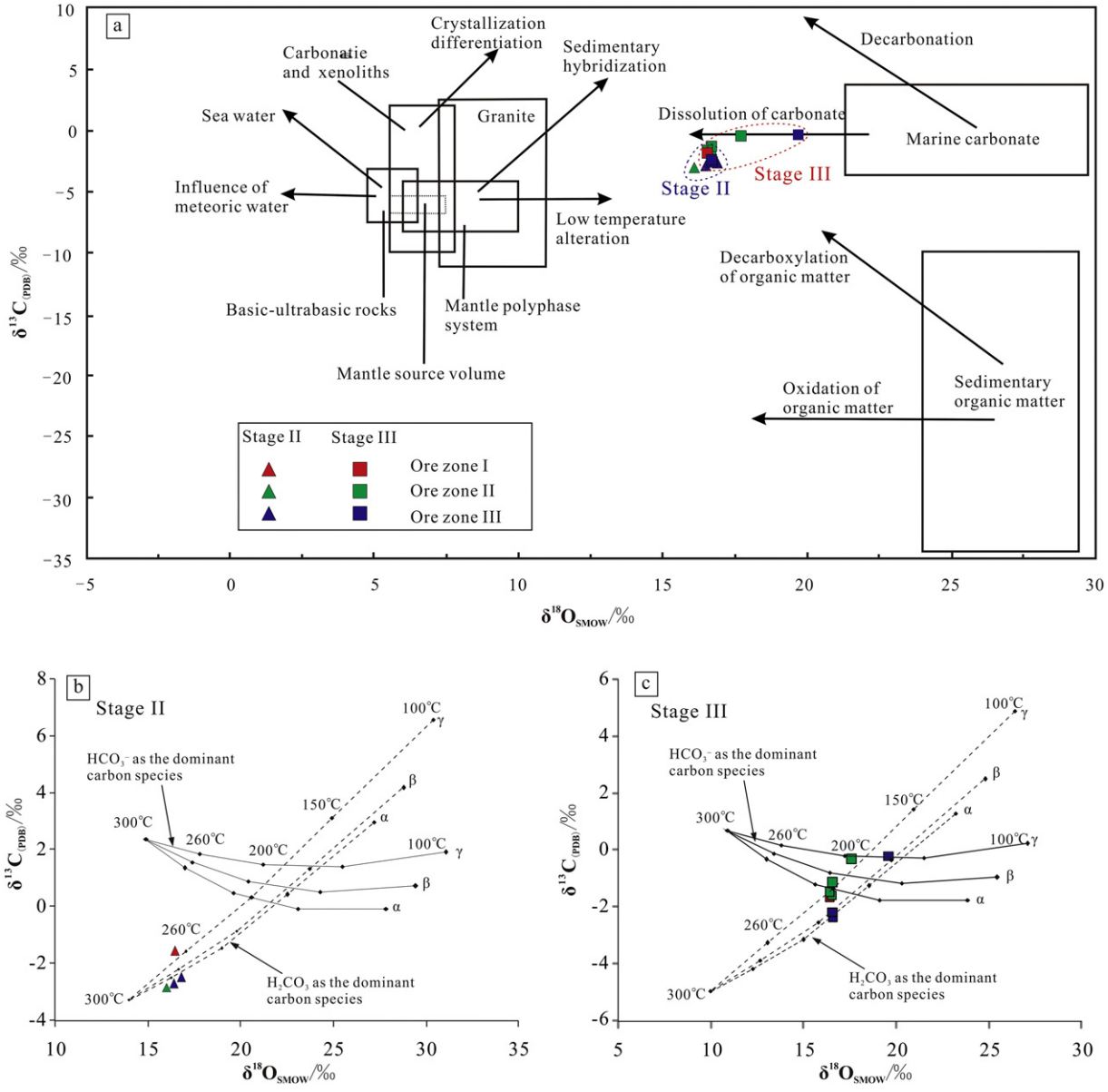

Fig. 15. Carbon and oxygen isotopes of calcite from the Huachanggou gold deposits. a. $\delta^{18}O$ vs. $\delta^{13}C$ diagram (after Liu and Liu, 1997; Liu et al., 2004). b. Water–rock interaction modeling for the stage II, with initial $\delta^{13}C = -2‰$ and $\delta^{18}O = 10‰$ for fluid. c. Water–rock interaction modeling for the stage III, with initial $\delta^{13}C = -4‰$ and $\delta^{18}O = 6‰$ for fluid. α – $\Delta^{13}C^{i}_{f} = 0.5‰$, $\Delta^{18}O^{i}_{f} = 2‰$; β – $\Delta^{13}C^{i}_{f} = 1.5‰$, $\Delta^{18}O^{i}_{f} = 4‰$; γ – $\Delta^{13}C^{i}_{f} = 3.5‰$, $\Delta^{18}O^{i}_{f} = 6‰$.

geological processes are shown as arrows in Fig. 15a (Dai, 1988; Dai and Chen, 1993; Liu and Liu, 1997; Liu et al., 2004). The values of calcite from the Huachanggou gold deposit are plotted near the area of marine carbonate and along the arrow of dissolution of carbonate. This variation in isotopic composition indicates that the carbon in the deposit was derived from the dissolution of marine carbonate.

The water–rock interaction can also simulate the evolution of the carbon and oxygen isotopic composition (Zheng and Hoefs, 1993; Liu et al., 2004; Long et al., 2009). The carbon and oxygen isotopic composition of calcite is related to temperature and rock/water value (R/W) (Taylor, 1974; Zheng, 1990; Zheng and Hoefs, 1993):

$$\delta^{13}C_{calcite} = \delta^{13}C^{i}_{water} + \Delta^{13}C^{calcite}_{water} + (R/W)\cdot\Delta^{13}C^{i}_{f},$$

$$\delta^{18}O_{calcite} = \delta^{18}O^{i}_{water} + \Delta^{18}O^{calcite}_{water} + (R/W)\cdot\Delta^{18}O^{i}_{f},$$

where $\Delta^{i}_{f} = \delta^{i}_{rock} - \delta^{f}_{rock}$. Normally, only small amount of CH_4 and CO_3^{2-} occur in hydrothermal fluids, and the isotopic fractionation between calcite and fluid is determined by the proportion of H_2CO_3 (including CO_2) and HCO_3^- in fluids (Zheng and Hoefs, 1993):

$$\Delta^{13}C^{calcite}_{water} = \Delta^{13}C^{calcite}_{CO_2} - x_{HCO_3^-}\cdot\Delta^{13}C^{HCO_3^-}_{CO_2},$$

$$\Delta^{18}O^{calcite}_{water} = \Delta^{18}O^{calcite}_{H_2O} - x_{CO_2}\cdot\Delta^{18}O^{CO_2}_{H_2O},$$

where Δ^{a}_{b} represents the value of isotopic fractionation between a and b which is calculated by equations from O'Neil et al. (1969), Rye and Ohmoto (1974), Truesdell (1974) and Ohmoto and Rye (1979); x_{CO_2} and $x_{HCO_3^-}$ represent the proportions of H_2CO_3 (including CO_2) and HCO_3^- in fluid, respectively.

The theoretical curves for either H_2CO_3 or HCO_3^- as the dominant dissolved carbon species in fluid are calculated with R/W value varying from 0 to 1 and temperature decreasing from 300 °C to 100 °C (Fig. 15b, c). If HCO_3^- is the dominant species of dissolved carbon in the fluid, the precipitated calcite will show a small variation in $\delta^{13}C$

values relative to temperature but a larger variation in $\delta^{18}O$ values (Zheng and Hoefs, 1993). If H_2CO_3 is the dominant species, calcite will show a large variation in $\delta^{13}C$ but a smaller variation in $\delta^{18}O$.

For stage II, H_2CO_3 was the dominant species of dissolved carbon in the ore-forming fluid with initial $\delta^{13}C = -2‰$ and $\delta^{18}O = 10‰$, and the temperature of formation of calcite was 250–265 °C (Fig. 15b). For stage III, initial $\delta^{13}C$ and $\delta^{18}O$ of the ore-forming fluid were respectively −4‰ and 6‰, and calcite was precipitated at the temperature of 170 °C to 205 °C (Fig. 15c). These $\delta^{18}O$ values are close to the values calculated from the $\delta^{18}O$ value of quartz (8.8 − 11.6‰ for stage II and 1.3 − 6.8‰ for stage III).

In the deposit, the dissolved carbon in fluids was derived mainly from the dissolution of marine carbonate in the wall rocks. The average $\delta^{13}C$ value of marine carbonate is 0‰ (Clark and Fritz, 1997; Zheng and Chen, 2000), which is larger than the $\delta^{13}C$ value of the fluids of the deposit. In the circumstances, the $\delta^{13}C$ values of the fluids should increase with the dissolution of marine carbonate. On the contrary, the $\delta^{13}C$ values of the fluids decreased from −2‰ (stage II) to −4‰ (stage III). This decrease is best interpreted as the mixing with a fluid with lower $\delta^{13}C$ value. Considering that seawater, magmatic water and meteoric water exhibit average $\delta^{13}C$ values of 0‰, −5‰ and −7‰, respectively, (Zheng and Hoefs, 1993; Clark and Fritz, 1997; Zheng and Chen, 2000), the decrease of fluid $\delta^{13}C$ value indicates the mixing with meteoric water.

5.5. Mechanism of ore-formation

The Huachanggou gold deposit is considered to be an orogenic gold deposit, the characteristics of which are similar to those of typical examples (Chen et al., 2004; Groves et al., 2003; Goldfarb et al., 2005; Chen, 2010; Liu et al., 2015a): (1) the deposit occupies a spatial and temporal position consistent with the Qinling Orogen which is a collisional orogenic belt; (2) the wall rocks were deformed and metamorphosed to phyllite; (3) mineralization is structurally controlled by ductile shear zone; (4) pyrite is the dominant sulfide mineral in the ores; (5) the ores exhibit a simple element assemblage of Au–Ag, and gold occurs in the form of native gold which is mainly microscopic and visible; (6) gold was deposited from moderate–low-salinity, salt solution–CO_2 hydrothermal fluid at medium temperature; (7) carbon was derived from the dissolution of marine carbonate and sulfur from the reduction of seawater sulfate; and (8) the ore-forming fluid had a metamorphic source.

Some orogenic gold deposits are associated with granitoids (Qiu et al., 2002; Yang et al., 2012a). In the Huachanggou area, the only magmatic rock is spilite which is one of the important host rocks to the gold mineralization. Spilite yields a SHRIMP U–Pb age of 801. 7 ± 4.7 Ma, which indicates that the Neoproterozoic spilite together with the Devonian sedimentary strata formed a tectonic mélange produced by the closure of the Mian–Lue Ocean (Lin et al., 2013). The gold mineralization event took place far later than the formation of spilite and was not directly related to the spilitic magmatic event. Notwithstanding, spilite provided part of ore-forming materials for the gold mineralization.

The Devonian stratum with a high gold content created the conditions for the preconcentration of gold. Following the closure of the Mian–Lue Ocean during the Indosinian period, the tectonic setting transitioned from oceanic slab subduction to intercontinental collision (Chen, 2010; Dong et al., 2011), and inevitably, collisional orogenic event triggered the large-scale imbricate nappe structures and deep-sourced metamorphic fluid which were associated with dehydration and decarbonization. The tectonic thermal effect and geothermal gradient were the two main factors which constrained the migration of ore-forming fluids and metals (Liu et al., 2015a,b). Owing to the mixing with meteoric water and the sudden change of physico-chemical conditions (e.g., temperature, pressure and redox potential), sulfides precipitated from the fluids, and gold enrichment in suitable spaces was produced by deformation (e.g., the tension fissures in spilite and the unconformity surface and formation interface of limestone and phyllite).

In the Huachanggou gold deposit, gold precipitated mainly during stage II. Physicochemical condition can be estimated from the phase stability relationships in stage II veins using Log $f(O_2)$ vs. pH diagram at 260 °C (Fig. 16). The shaded area is defined by the coexistence of pyrite, chalcopyrite and calcite, as well as sericite and galena. The diagram indicates a pH value of 4.5–5.8. Given that the pH value of water is around 5.3 at 260 °C and 100 Mpa (Liu, 2011), the ore-forming fluid of the deposit was near-neutral. In near-neutral reduced fluid, $HAu(HS)_2$ or $Au(HS)_2^-$ is the dominant gold-bearing species under conditions where $m(\Sigma SO_4^{2-}) < m(H_2S)$ at most conditions where pyrite is stable as the main Fe-bearing minerals (Hayashi and Ohmoto, 1991; Cooke et al., 1996). Because the calcite-gold mineral assemblage was more consistent with weak alkaline condition, $Au(HS)_2^-$ was probably the dominant auriferous complex during gold migration in the Huachanggou gold deposit (Fig. 16). The solubility of gold in the form of $Au(HS)_2^-$ changes slightly with the decrease of temperature (Cooke et al., 1996), and thereby $Au(HS)_2^-$ could transport a large quantity of gold into the cooler parts of the Huachanggou fluid system. Gold solubility in H_2S-rich fluid is controlled by:

$$Au(HS)_2^- + 0.5H_2 + H^+ = Au^0 + 2H_2S.$$

In the Huachanggou gold deposit, H_2S was the dominant sulfur-bearing species, thus both the increase of $Au(HS)_2^-$ and H_2 contents and the decrease of ΣS and pH values could trigger the precipitation of

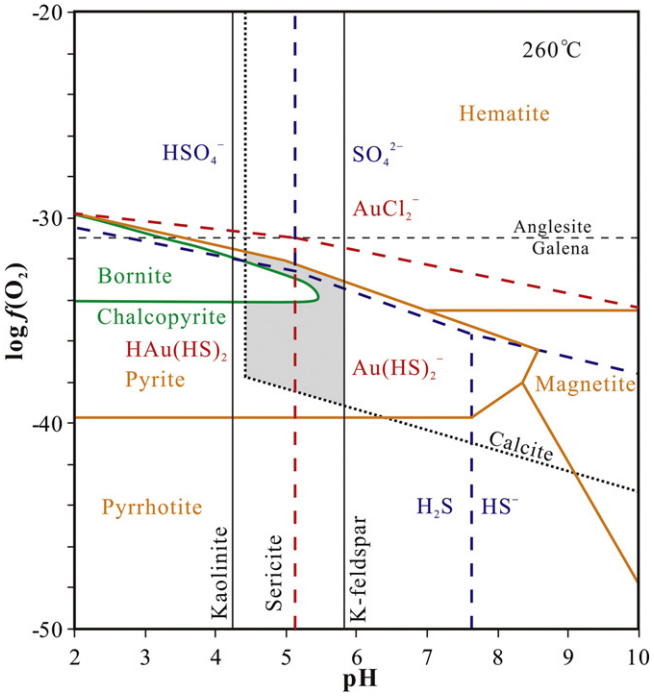

Fig. 16. Log $f(O_2)$ vs pH diagram, showing approximate conditions of stage II fluid relative to mineral stability in Fe–Cu–O–S system at 260 °C with a salinity of 6.5 wt.% NaCl equiv, $\Sigma S = 0.01$ m, and $\Sigma C = 1$ m. The temperature and salinity are set according to the study on pyrite and fluid inclusions. ΣS and ΣC values are appropriate to hydrothermal based, precious metal fluids (Zhang and Spry, 1994). The shaded area represents the estimated conditions for stage II sulfide mineralization. The orange and black solid lines represent boundaries of Fe–Cu–O–S minerals, and kaolinite, sericite, and K-feldspar equilibrium, respectively; the dark blue line represents the limit of calcite (Dai and Liu, 1994; Zhang and Spry, 1994). The black dashed line represents the boundary of anglesite and galena equilibrium calculated using thermodynamic data from Cooke et al., 1996. The red and blue dashed lines represent the predominance fields of $Au(HS)_2^-$, $HAu(HS)_2$, and $AuCl_2^-$, and aqueous sulfur-bearing species (Hayashi and Ohmoto, 1991; Cooke et al., 1996).

gold. Chemical equations for the formation process of pyrite (FeS_2) are as follows:

$$2H_2S + Fe^{2+} = FeS_2 + 2H^+ + H_2,$$

$$2HS^- + Fe^{2+} = FeS_2 + H_2.$$

The precipitation of pyrite can trigger the decrease of ΣS and pH values and the increase of H_2 content, and the precipitation of gold based on this reaction (Goldfarb et al., 2005; Large et al., 2011):

$$Fe^{2+} + 2Au(HS)_2^- + 2H_2 = FeS_2 + Au^0 + 2H_2S.$$

The massive sulfidation of dissolved Fe is an important factor for the precipitation of gold. The ore-forming fluid of the Huachanggou gold deposit had experienced boiling. The boiling of fluid triggered a large scale of precipitation of metal sulfides, and it was an effective depositional mechanism for gold precipitation in the Huachanggou hydrothermal system.

6. Conclusions

(1) The Huachanggou gold deposit is considered to be an orogenic gold deposit.
(2) The deposit exhibits a simple ore-forming element group of Au–Ag.
(3) The ore-forming fluid was derived originally from metamorphic fluid, and the ore-forming elements were derived mainly from the wall rocks.
(4) Au migrated mainly in the form of $Au(HS)_2^-$ to form the Huachanggou gold deposit. The boiling of fluid triggered the precipitation of metal sulfides and gold.

Acknowledgments

Funding for this project was jointly granted by the Key Program of National Natural Science Foundation of China (Grant No. 41030423), by the Major Basic Research Program of People's Republic of China (Grant No. 2014CB440903), by the Specialized Research Fund for the Doctoral Program of Higher Education (Grant No. 20130022110001), by the National Natural Science Foundation of China (Grant Nos. 41173062 and 40972071), by the work items of China Geological Survey (Grant Nos. 1212011220924 and 1212011120354), and by the 111 Project under the Ministry of Education and the State Administration of Foreign Experts Affairs, China (Grant No. B07011). We are grateful to Huachanggou Gold Mine Co. Ltd. for the support and Engineer Kangwei Yu for the enthusiastic help during fieldwork. This manuscript has also benefited from the comments and critical reviews from Managing Editor Peter C. Lightfoot and two anonymous reviewers. Editor-in-Chief Franco Pirajno has also handled the manuscript.

References

Arribas, A., Cunningham, C.G., Rytuba, J.J., Rye, R.O., Kelly, W.C., Podwysocki, M.H., Mckee, E.H., Tosdal, R.M., 1995. Geology, geochronology, fluid inclusions, and isotope geochemistry of the Rodalquilar gold alunite deposit, Spain. Econ. Geol. 90, 795–822. http://dx.doi.org/10.2113/gsecongeo.90.4.795.

Bai, Z., 1996a. Genesis of the Huachanggou gold deposit in Shanxi province. Miner. Resour. Geol. 10, 108–113 (in Chinese with English abstract).

Bai, Z., 1996b. Geology and genesis of the Huachanggou gold deposit in Shanxi province. Northwest. Geol. 17, 16–23 (in Chinese with English abstract).

Bodnar, R.J., 1993. Revised equation and table for determining the freezing point depression of H_2O–NaCl solutions. Geochim. Cosmochim. Acta 57, 683–684. http://dx.doi.org/10.1016/0016-7037(93)90378-A.

Bovik, A., Huang, T.S., Munson Jr., D., 1983. A generalization of median filtering using linear combinations of order statistics. IEEE Trans. Acoust. Speech Signal Process. 31, 1342–1349. http://dx.doi.org/10.1109/TASSP.1983.1164247.

Bur, T., Probst, M., Neguessan, M., Probst, A., 2009. Distribution and origin of lead in stream sediments from small agricultural catchments draining Miocene molassic deposits (SW France). Appl. Geochem. 24, 1324–1338. http://dx.doi.org/10.1016/j.apgeochem.2009.04.004.

Chang, Z.S., Large, R.R., Maslennikov, V., 2008. Sulfur isotopes in sediment-hosted orogenic gold deposits: evidence for an early timing and a seawater sulfur source. Geology 36, 971–974. http://dx.doi.org/10.1130/G25001A.1.

Chen, Y.J., 2010. Indosinian tectonic setting, magmatism and metallogenesis in Qinling Orogen, Central China. Geol. China 37, 854–865 (in Chinese with English abstract).

Chen, J.S., Chu, X.L., 1988. Sulfur isotope composition of Triassic marine sulfates of South China. Chem. Geol. 72, 155–161.

Chen, Y.J., Zhang, J., Zhang, F.X., Pirajno, F., Li, C., 2004. Carlin and Carlin-like gold deposits in western Qinling Mountains and their metallogenic time, tectonic setting and model. Geol. Rev. 50, 134–152 (in Chinese with English abstract).

Chen, Y.J., Ni, P., Fan, H.R., Pirajno, F., Lai, Y., Su, W.C., Zhang, H., 2007. Diagnostic fluid inclusions of different types hydrothermal gold deposits. Acta Petrol. Sin. 23, 2085–2108 (in Chinese with English abstract).

Chen, H.Y., Li, S.R., Zhang, X.B., Zhou, Q.F., Zhang, Y.Q., Liu, Z.H., Zhang, H.F., Wang, N., 2010. Thermoelectric character of pyrite from Jinqingding gold deposit in eastern Shandong Province and its significance. Mineral Deposits 29, 1125–1137 (in Chinese with English abstract).

Chernyshev, I.V., Bortnikov, N.S., Chugaev, A.V., Gamyanin, G.N., Bakharev, A.G., 2011. Metal sources of the large Nezhdaninsky orogenic gold deposit, Yakutia, Russia: results of high-precision MC-ICP-MS analysis of lead isotopic composition supplemented by data on strontium isotopes. Geol. Ore Deposits 53, 353–373. http://dx.doi.org/10.1134/S1075701511050035.

Chester, R., Stoner, C., 1973. Pb in particulates from the lower atmosphere of the eastern Atlantic. Nature 245, 27–28. http://dx.doi.org/10.1038/245027b0.

Chugaev, A.V., Plotinskaya, O.Yu., Chernyshev, I.V., Kotov, A.A., 2014. Lead isotope heterogeneity in sulfides from different assemblages at the Verninskoe gold deposit (Baikal-Patom Highland, Russia). Dokl. Earth Sci. 457, 887–892. http://dx.doi.org/10.1134/S1028334X14070216.

Clark, I., Fritz, P., 1997. Environmental Isotopes in Hydrogeology. Lewis Publishers, New York, p. 328.

Claypool, G.E., Holser, W.T., Kaplan, I.R., Sakai, H., Zak, I., 1980. The age curves of sulfur and oxygen isotopes in marine sulfate and their mutual interpretation. Chem. Geol. 28, 199–260. http://dx.doi.org/10.1016/0009-2541(80)90047-9.

Clayton, R.N., Mayeda, T.K., 1963. The use of bromine pentafluoride in the extraction of oxygen from oxides and silicates for isotopic analysis. Geochim. Cosmochim. Acta 27, 43–52. http://dx.doi.org/10.1016/0016-7037(63)90071-1.

Clayton, R.N., O'Neil, J.R., Mayeda, T.K., 1972. Oxygen isotope exchange between quartz and water. J. Geophys. Res. 77, 3057–3067. http://dx.doi.org/10.1029/JB077i017p03057.

Coleman, M.L., Sheppard, T.J., Durham, J.J., Rouse, J.E., Moore, G.R., 1982. Reduction of water with zinc for hydrogen isotope analysis. Anal. Chem. 54, 993–995. http://dx.doi.org/10.1021/ac00243a035.

Collins, P.L.F., 1979. Gas hydrates in CO_2-bearing fluid inclusions and use of freezing data for estimation of salinity. Econ. Geol. 74, 1435–1444. http://dx.doi.org/10.2113/gsecongeo.74.6.1435.

Cooke, D.R., McPhail, D.C., Bloom, M.S., 1996. Epithermal gold mineralization, Acupan, Baguio district, Philippines: geology, mineralization, alteration, and the thermochemical environment of ore deposition. Econ. Geol. 91, 243–272. http://dx.doi.org/10.2113/gsecongeo.91.2.243.

Dai, J.X., 1988. Carbon isotopic composition characteristics and origin of natural gases at Liuhuangtang, Tengchong County, Yunnan Province. Chin. Sci. Bull. 33, 1168–1170 (in Chinese with English abstract).

Dai, J.X., Chen, Y., 1993. Carbon isotopic characteristics of alkane fraction in biogenic gases in China and their discriminating indicators. Sci. China B 23, 303–305 (in Chinese with English abstract).

Dai, S.B., Liu, L.D., 1994. Recent development of the study of physic–chemical conditions during gold mineralization. J. Prec. Met. Geol. 3, 65–73 (in Chinese with English abstract).

Das, S.K., Routh, J., Roychoudhury, N., Klump, J.V., 2008. Major and trace element geochemistry in Zeekoevlei, Southern Africa: a lacustrine record of present and past processes. Appl. Geochem. 23, 2496–2511. http://dx.doi.org/10.1016/j.apgeochem.2008.02.011.

Dong, H., 2004. Disintegration of the "Sanhekou Group" of the Sanhekou area, Southern Qinling and its age. J. Stratigr. 28, 59–63 (in Chinese with English abstract).

Dong, Y.P., Zhang, G.W., Neubauer, F., Liu, X.M., Genser, J., Hauzenberger, C., 2011. Tectonic evolution of the Qinling orogen, China: review and synthesis. J. Asian Earth Sci. 41, 213–237. http://dx.doi.org/10.1016/j.jseaes.2011.03.002.

Du, Y.S., Sheng, J.H., Feng, Q.L., Gu, S.Z., Chen, J.Y., Yang, Y.C., Li, R.S., 1998. Disintegration of the "Sanhekou Group" in the Mianxian–Lueyang area, South Qinling and its geological significance. J. Stratigr. 22, 170–175 (in Chinese with English abstract).

Feng, J.Z., Shao, S.C., Wang, D.B., Wang, X.M., Ma, Z.G., 2002. Baguamiao superlarge gold deposit in the Qinling orogen: the characteristics of its control by the brittle–ductile shear zone and dynamic mechanism for ore-forming structure. Geol. China 29, 58–66 (in Chinese with English abstract).

Feng, J.Z., Wang, D.B., Wang, X.M., Shao, S.C., Lin, G.F., Shi, J.J., 2003. Geology and metallogenesis of Liba large-size gold deposit in Lixian, Gansu Province. Mineral Deposits 22, 257–263 (in Chinese with English abstract).

Fouillac, A.M., Javoy, M., 1988. Oxygen and hydrogen isotopes in the volcano-sedimentary complex of Huelva (Iberian Pyrite Belt): example of water circulation through a volcano-sedimentary sequence. Earth Planet. Sci. Lett. 87, 473–484. http://dx.doi.org/10.1016/0012-821X(88)90010-6.

Friedman, I., O'Neil, J.R., 1977. Compilation of stable isotope fractionation factors of geochemical interest. In: Fleischer, M. (Ed.), Data of Geochemistry, 6th ed. U.S. Geological Survey Professional Paper vol. 440–KK. United States Government Printing Office, Washington, pp. KK1–KK12 (Reston, VA).

Glesemann, A., Jäger, H.J., Norman, A.L., Krouse, H.R., Brand, W.A., 1994. Online sulfur isotope determination using an elemental analyser coupled to a mass spectrometer. Anal. Chem. 66, 2816–2819. http://dx.doi.org/10.1021/ac00090a005.

Goldfarb, R.J., Baker, T., Dube, B., Groves, D.I., Hart, C.J.R., Gosselin, P., 2005. Distribution, character, and genesis of gold deposits in metamorphic terranes. In: Hedenquist, J.W., Thompson, J.F.H., Goldfarb, R.J., Richards, J.P. (Eds.), Econ. Geol 100th Anniversary vol. Society of Economic Geologists, Littleton, US, pp. 407–450.

Goldfarb, R.J., Taylor, R.D., Collins, G.S., Goryachev, N.A., Orlandini, O.F., 2014. Phanerozoic continental growth and gold metallogeny of Asia. Gondwana Res. 25, 48–102. http://dx.doi.org/10.1016/j.gr.2013.03.002.

Gomes, A., Ares, J.R., Ferrer, I.J., da Silva Pereira, M.I., Sánchez, C., 2003. Formation of n-type pyrite films from electrodeposited iron sulphides: effect of annealing temperature. Mater. Res. Bull. 38, 1123–1133. http://dx.doi.org/10.1016/S0025-5408(03)00116-8.

Groves, D.I., Goldfarb, R.J., Gebre-Mariam, M., Hagemann, S.G., Robert, F., 1998. Orogenic gold deposits: a proposed classification in the context of their crustal distribution and relationship to other gold deposit types. Ore Geol. Rev. 13, 7–27. http://dx.doi.org/10.1016/S0169-1368(97)00012-7.

Groves, D.I., Goldfarb, R.J., Robert, F., Hart, C.J.R., 2003. Gold deposits in metamorphic belts: overview of current understanding, outstanding problems, future research, and exploration significance. Econ. Geol. 98, 1–29. http://dx.doi.org/10.2113/98.1.1.

Gulson, B.L., 1986. Lead Isotopes in Mineral Exploration. Elsevier, Amsterdam and New York, pp. 1–245.

Guo, L.N., Zhang, C., Song, Y.Z., Chen, B.H., Zhou, Z., Zhang, B.L., Xu, X.L., Wang, Y.W., 2014. Hydrogen and oxygen isotopes geochemistry of the Wang'ershan gold deposit, Jiaodong. Acta Petrol. Sin. 30, 2481–2494 (in Chinese with English abstract).

Hansmann, W., Koppel, V., 2000. Lead-isotopes as traces of pollutants in soils. Chem. Geol. 171, 123–144. http://dx.doi.org/10.1016/S0009-2541(00)00230-8.

Harlavan, Y., Erel, Y., Blum, J.D., 1998. Systematic changes in lead isotopic composition with soil age in glacial granitic terrains. Geochim. Cosmochim. Acta 62, 33–46. http://dx.doi.org/10.1016/S0016-7037(97)00328-1.

Harrison, A.G., Thode, H.G., 1957. The kinetic isotope effect in the chemical reduction of sulphate. Trans. Faraday Soc. 53, 1648–1651. http://dx.doi.org/10.1039/TF9575301648.

Hayashi, K.I., Ohmoto, H., 1991. Solubility of gold in NaCl- and H_2S-bearing aqueous solutions at 250–350 °C. Geochim. Cosmochim. Acta 55, 2111–2126. http://dx.doi.org/10.1016/0016-7037(91)90091-I.

Hoefs, J., 1997. Stable Isotope Geochemistry. 4th ed. Springer Verlag, Berlin, pp. 65–168.

Hofstra, A.H., Cline, J.S., 2000. Characteristics and models for Carlin-type gold deposits. In: Hagemann, S.G., Brown, P.E. (Eds.), Gold in 2000. Rev. Econ. Geol 13, pp. 163–220.

Hollister, V.F., 1985. Discoveries of epithermal precious metal deposits. Society of Mining Engineers of the American Institute of Mining, Metallurgical, and Petroleum Engineers, New York (169 pp.).

Holser, W.T., Magaritz, M., Ripperdan, R.L., 1996. Global isotopic events. In: Walliser, O.H. (Ed.), Global Events and Event Stratigraphy in the Phanerozoic. Springer, Berlin Heidelberg, pp. 63–88.

Hu, C.Y., 2001. Characteristics of trace elements, thermoelectricity and crystal form of pyrite. Geoscience 15, 238–241 (in Chinese with English abstract).

Hu, R.Z., Su, W.C., Bi, X.W., Tu, G.Z., Hofstra, A.H., 2002. Geology and geochemistry of Carlin-type gold deposits in China. Mineral. Deposita 37, 378–392. http://dx.doi.org/10.1007/s00126-001-0242-7.

Jiang, Y.H., Jin, G.D., Liao, S.Y., Zhou, Q., Zhao, P., 2010. Geochemical and Sr–Nd–Hf isotopic constraints on the origin of Late Triassic granitoids from the Qinling orogen, central China: implications for a continental arc to continent–continent collision. Lithos 117, 183–197. http://dx.doi.org/10.1016/j.lithos.2010.02.014.

Jiang, S.H., Wang, C.M., Zhao, H., He, X.Y., Xia, R., Guo, C.Y., Lai, X.R., Ouyang, X.C., 2015. Geochemical characteristics of stable isotopes and metallogenic material source in the Xincheng gold deposit. Geol. Explor. 51, 68–78 (in Chinese with English abstract).

Johnson, A.R., Wichern, W.D., 1988. Applied Multivariate Statistical Analysis. second ed. Prentice-Hall, Englewood Cliffs, NJ, p. 607.

Kesler, S.E., Fortuna, J., Ye, Z., Alt, J., Core, D.P., Zohar, P., Borhauer, J., Chryssoulis, S.L., 2003. Evaluation of the role of sulfidation in deposition of gold, Screamer section of the Betze–Post Carlin-type deposit, Nevada. Econ. Geol. 98, 1137–1157. http://dx.doi.org/10.2113/gsecongeo.98.6.1137.

Large, R.R., Bull, S.W., Maslennikov, V.V., 2011. A carbonaceous sedimentary source-rock model for Carlin-type and orogenic gold deposits. Econ. Geol. 106, 331–358. http://dx.doi.org/10.2113/econgeo.106.3.331.

Lerch, M.F., Xue, F., Kröner, A., Zhang, G.W., Todt, W., 1995. A Middle Silurian–Early Devonian magmatic arc in the Qinling Mountains of central China. J. Geol. 103, 437–449 (Stable URL: http://www.jstor.org/stable/30071164).

Li, H.A., Tai, Y.H., 2007. Geological characteristics and genesis of gold deposits in Huachanggou mine. Nonferrous Metals 59, 23–26 (in Chinese with English abstract).

Li, S.R., Chen, G.Y., Shao, W., Sun, D.S., 1996a. Genetic Mineralogy of Rushan Gold deposit in Jiaodong Peninsula. Geological Publishing House, Beijing, pp. 98–101 (in Chinese).

Li, S.G., Sun, W.D., Zhang, G.W., Chen, J.Y., Yang, Y.C., 1996b. Chronology and geochemistry of metavolcanic rocks from Heigouxia valley in the Mian–Lue tectonic zone, south Qinling–Evidence for a Paleozoic oceanic basin and its close time. Sci. China Ser. D Earth Sci. 39, 300–310.

Li, H., Zheng, T., Tang, L., Hui, D.F., Shi, J.H., Wu, J.X., Wang, L.F., Cheng, J.J., Lin, L.H., 2000. The model of superimposed primary halos in shuangwang gold deposit, Shaanxi. J. Guilin Inst. Technol. 20, 327–333 (in Chinese with English abstract).

Li, B., Li, M.J., Wang, Y.L., Liu, F.Q., Xiao, H., Lin, Y.C., Li, Y.Y., Liu, F.F., Wang, Q.L., 2014. Detailed Survey Report of the Huachanggou Gold Deposit. Huachanggou Gold Mine Co. Ltd., Lueyang (in Chinese; unpublished).

Lin, Z.W., Qin, Y., Yue, S.W., Zhou, Z.J., Wang, L.X., 2011. The study of zircon U–Pb geochronology from quartz veins in the Huachanggou gold deposit, Shaanxi Province. Acta Mineral. Sin. 31, 614–615 (in Chinese).

Lin, Z.W., Qin, Y., Zhou, Z.J., Yue, S.W., Zeng, Q.T., Wang, L.X., 2013. Zircon U–Pb dating and geochemistry of the volcanic rocks at Huachanggou area, Mian–Lue suture, South Qinling. Acta Petrol. Sin. 29, 83–94 (in Chinese with English abstract).

Lin, X., Wang, X.Q., Zhang, B.M., Yao, W.S., 2014. Multivariate analysis of regolith sediment geochemical data from the Jinwozi gold field, north-western China. J. Geochem. Explor. 137, 48–54. http://dx.doi.org/10.1016/j.gexplo.2013.11.006.

Liu, B., 2011. Calculation of pH and Eh for aqueous inclusions as simple system. Acta Petrol. Sin. 27, 1533–1542 (in Chinese with English abstract).

Liu, J.M., Liu, J.J., 1997. Basinal fluid genetic model of fine disseminated gold deposits in the Golden Triangle area between Yunnan, Guizhou and Guangxi. Acta Mineral. Sin. 17, 448–456 (in Chinese with English abstract).

Liu, J.J., Zheng, M.H., Zhou, D.A., Liu, J.M., Zhou, Y.F., 1998. The components and evolution of the hydrogen and oxygen isotopes of ore-forming fluids form La'erma gold ore belt. J. Changchun Univ. Sci. Technol. 28, 43–49 (in Chinese with English abstract).

Liu, J.J., He, M.Q., Li, Z.M., Liu, Y.P., Li, C.Y., Zhang, Q., Yang, W.G., Yang, A.P., 2004. The oxygen and carbon isotopic geochemistry and its significance in Baiyangping silver copper polymetallic metallogenic concentration area, Lanping Basin. Mineral Deposits 23, 1–10 (in Chinese with English abstract).

Liu, J.J., Mao, G.J., Wu, S.H., Wang, J.P., Ma, X.H., Li, L.X., Liu, G.Z., Liao, Y.F., Zheng, W.J., 2010. Metallogenic characteristics and formation mechanism of Zhaishang gold deposit, southern Gansu Province. Mineral Deposits 29, 85–100 (in Chinese with English abstract).

Liu, C.H., Liu, J.J., Wang, J.P., Yang, L.B., Wang, W.Y., Wang, L.X., Yu, K.W., Wang, L.T., 2012. The primary halo research of the main ore zone in the Huachanggou gold deposit in Lueyang, Shaanxi Province. Geol. China 39, 1397–1405 (in Chinese with English abstract).

Liu, C.H., Liu, J.J., Wang, J.P., Wang, W.Y., Wang, L.X., Yu, K.W., Chen, D., Li, Z.G., 2013a. The primary halo research of the main ore zone In the Huachanggou gold deposit in Lueyang, Shaanxi Province. Geoscience 27, 1–12 (in Chinese with English abstract).

Liu, C.H., Liu, J.J., Wang, J.P., Yang, L.B., Wu, J., Jia, L., 2013b. Geochemical characteristics of rare earth elements and their implications for the Huachanggou gold deposit in Shaanxi Province, China. J. Rare Earths 31, 215–226. http://dx.doi.org/10.1016/S1002-0721(12)60261-0.

Liu, J.J., Liu, C.H., Carranza, E.J.M., Li, Y.J., Mao, Z.H., Wang, J.P., Wang, Y.H., Zhang, J., Zhai, D.G., Zhang, H.F., Shan, L., Zhu, L.M., Lu, R.K., 2015a. Geological characteristics and ore-forming process of the gold deposits in the western Qinling region, China. J. Asian Earth Sci. 103, 40–69. http://dx.doi.org/10.1016/j.jseaes.2014.11.012.

Liu, J.J., Dai, H.Z., Zhai, D.G., Wang, J.P., Wang, Y.H., Yang, L.B., Mao, G.J., Liu, X.H., Liao, Y.F., Yu, C., Li, Q.Z., 2015b. Geological and geochemical characteristics and formation mechanisms of the Zhaishang Carlin-like type gold deposit, western Qinling Mountains, China. Ore Geol. Rev. 64, 273–298. http://dx.doi.org/10.1016/j.oregeorev.2014.07.016.

Long, H.S., Luo, T.Y., Huang, Z.L., Zhou, M.Z., Yang, Y., Qian, Z.K., 2009. Carbon and oxygen isotopic geochemistry of Laochang large-sized Ag polymetallic deposit in Lancang, Yunnan Province and its significance. Mineral Deposits 28, 687–695 (in Chinese with English abstract).

Luo, B.J., Zhang, H.F., Lü, X.B., 2012. U–Pb zircon dating, geochemical and Sr–Nd–Hf isotopic compositions of Early Indosinian intrusive rocks in West Qinling, central China: petrogenesis and tectonic implications. Contrib. Mineral. Petrol. 164, 551–569. http://dx.doi.org/10.1007/s00410-012-0748-2.

Mao, J.W., Qiu, Y.M., Goldfarb, R.J., Zhang, Z.C., Garwin, S., Fengshou, R., 2002. Geology, distribution, and classification of gold deposits in the western Qinling belt, central China. Mineral. Deposita 37, 352–377. http://dx.doi.org/10.1007/s00126-001-0249-0.

Mao, J.W., Li, X.F., Li, H.M., Qu, X.M., Zhang, C.Q., Xue, C.J., Wang, Z.L., Yu, J.J., 2005. Types and characteristics of endogenetic metallic deposits in orogenic belts in China and their metallogenic processes. Acta Geol. Sin. 79, 342–371 (in Chinese with English abstract).

Mao, J.W., Zhou, Z.H., Feng, C.Y., Wang, Y.T., Zhang, C.Q., Peng, H.J., Yu, M., 2012. A preliminary study of the Triassic large-scale mineralization in China and its geodynamic setting. Geol. China 39, 1437–1471 (in Chinese with English abstract).

McCrea, J.M., 1950. The isotopic chemistry of carbonates and a paleotemperature scale. J. Chem. Phys. 18, 849–857. http://dx.doi.org/10.1063/1.1747785.

Meng, Q.R., Zhang, G.W., 1999. Timing of the collision of the North and South China blocks: Controversy and reconciliation. Geology 27, 123–126. http://dx.doi.org/10.1130/0091-7613(1999)027<0123:TOCOTN>2.3.CO;2.

Meng, Q.R., Zhang, G.W., 2000. Geologic framework and tectonic evolution of the Qinling orogen, central China. Tectonophysics 323, 183–196. http://dx.doi.org/10.1016/S0040-1951(00)00106-2.

Munhá, J., Kerrich, R., 1980. Sea water basalt interaction in spilites from the Iberian Pyrite Belt. Contrib. Mineral. Petrol. 73, 191–200. http://dx.doi.org/10.1007/BF00371394.

Nesbitt, H.W., Markovics, G., 1997. Weathering of granodioritic crust, long-term storage of elements in weathering profiles, and petrogenesis of siliciclastic sediments. Geochim. Cosmochim. Acta 61, 1653–1670. http://dx.doi.org/10.1016/S0016-7037(97)00031-8.

O'Neil, J.R., Clayton, R.N., Mayeda, T., 1969. Oxygen isotope fractionation in divalent metal carbonates. J. Chem. Phys. 51, 5547–5558. http://dx.doi.org/10.1063/1.1671982.

Ohmoto, H., 1972. Systematics of sulfur and carbon isotopes in hydrothermal ore deposits. Econ. Geol. 67, 551–578. http://dx.doi.org/10.2113/gsecongeo.67.5.551.

Ohmoto, H., Rye, R.O., 1979. Isotopes of sulfur and carbon. In: Barnes, H.L. (Ed.), Geochemistry of Hydrothermal Ore Deposits, 2nd ed. Wiley and Sons, New York, pp. 509–567.

Peng, B., Tang, X.Y., Yu, C.X., Tan, C.Y., Yin, C.Y., Yang, G., Liu, Q., Yang, K.S., Tu, X.L., 2011. Geochemistry of trace metals and Pb isotopes of sediments from the lowermost Xiangjiang River, Hunan Province (PR China): implications on sources of trace metals. Environ. Earth Sci. 64, 1455–1473. http://dx.doi.org/10.1007/s12665-011-0969-0.
Qiu, Y.M., Groves, D.I., McNaughton, N.J., Wang, L.G., Zhou, T.H., 2002. Nature, age, and tectonic setting of granitoid-hosted, orogenic gold deposits of the Jiaodong Peninsula, eastern North China craton, China. Mineral. Deposita 37, 283–305. http://dx.doi.org/10.1007/s00126-001-0238-3.
Ratschbacher, L., Hacker, B.R., Calvert, A., Webb, L.E., Grimmer, J.C., McWilliams, M.O., Ireland, T., Dong, S., Hu, J., 2003. Tectonics of the Qinling (Central China): tectonostratigraphy, geochronology, and deformation history. Tectonophysics 366, 1–53. http://dx.doi.org/10.1016/S0040-1951(03)00053-2.
Reed, M.F., Bartholomay, R.C., Hughes, S.S., 1997. Geochemistry and stratigraphic correlation of basalt lavas beneath the Idaho Chemical Processing Plant, Idaho National Engineering Laboratory. Environ. Geol. 30, 108–118. http://dx.doi.org/10.1007/s002540050138.
Rees, C.E., Jenkins, W.J., Monster, J., 1978. The sulphur isotopic composition of ocean water sulphate. Geochim. Cosmochim. Acta 42, 377–381. http://dx.doi.org/10.1016/0016-7037(78)90268-5.
Rollinson, H.R., 1993. Using Geochemistry Data: Evaluation, Presentation, Interpretation. Longman Scientific and Technical Ltd., Essex, pp. 1–352.
Rose, A.W., Hawkes, H.E., Webb, J.S., 1979. Geochemistry in Mineral Exploration. second ed. Academic Press Inc, London.
Rousseeuwa, P.J., Crouxa, C., 1993. Alternatives to the median absolute deviation. J. Am. Stat. Assoc. 88, 1273–1283. http://dx.doi.org/10.1080/01621459.1993.10476408.
Rye, R.O., Ohmoto, H., 1974. Sulfur and carbon isotopes and ore genesis: a review. Econ. Geol. 69, 826–842. http://dx.doi.org/10.2113/gsecongeo.69.6.826.
Schildlowski, M., 1998. Beginning of terrestrial life: problems of the early record and implications for extraterrestrial scenarios. Instruments, Methods, and Missions for Astrobiology, SPIE 3441, pp. 149–157 http://dx.doi.org/10.1117/12.319832.
Seal II, R.R., 2006. Sulfur isotope geochemistry of sulfide minerals. Rev. Mineral. Geochem. 61, 633–677. http://dx.doi.org/10.2138/rmg.2006.61.12.
Shao, W., Chen, G.Y., Sun, D.S., 1990. Study on thermoelectricity of pyrite and adhibition on gold deposit in Jiaodong region. Geoscience 4, 46–57 (in Chinese with English abstract).
Shen, W.Z., 1987. Stable Isotope Geochemistry. Atomic Energy Press, Beijing.
Shen, W.Z., Zhang, B.T., Ling, H.F., Lai, M.Y., Yang, J.D., Tan, X.C., 1991. Nd, Sr and O isotopic study on spilite–keratophyre in Xiqiu, Zhejiang Province. Acta Geol. Sin. 65, 337–346 (in Chinese with English abstract).
Shen, J.F., Li, S.R., Ma, G.G., Liu, Y., Yu, H.J., Liu, H.M., 2013. Typomorphic characteristics of pyrite from the Linglong gold deposit: Its vertical variation and prospecting significance. Earth Sci. Front. 20, 55–75 (in Chinese with English abstract).
Standisha, C.D., Dhuimea, B., Chapmanb, R.J., Hawkesworthc, C.J., Piked, A.W.G., 2014. The genesis of gold mineralisation hosted by orogenic belts: a lead isotope investigation of Irish gold deposits. Chem. Geol. 378–379, 40–51. http://dx.doi.org/10.1016/j.chemgeo.2014.04.012.
Taylor, H.P., 1974. The application of oxygen and hydrogen isotope studies to problems of hydrothermal alteration and ore deposition. Econ. Geol. 69, 843–883. http://dx.doi.org/10.2113/gsecongeo.69.6.843.
Truesdell, A.H., 1974. Oxygen isotope activities and concentrations in aqueous salt solutions at elevated temperatures: consequences for isotope geochemistry. Earth Planet. Sci. Lett. 23, 387–396. http://dx.doi.org/10.1016/0012-821X(74)90128-9.
Viets, J.G., Leach, D.L., 1990. Genetic implications of regional and temporal trends in ore fluid geochemistry of Mississippi Valley-type deposits in the Ozark region. Econ. Geol. 85, 842–861. http://dx.doi.org/10.2113/gsecongeo.85.4.842.
Webb, L.E., Hacker, B.R., Ratschbacher, L., Dong, S., 1999. Thermochronologic constraints on deformation and cooling history of high- and ultrahigh-pressure rocks in the Qinling–Dabie orogen, eastern China. Tectonics 18, 621–638. http://dx.doi.org/10.1029/1999TC900012.
Wei, G.F., Jiang, X.D., Liu, Y.H., Du, P.X., 2000. Geological characteristics and ore-controlling factors of the Huachanggou gold deposit. Mineral Deposits 19, 138–146 (in Chinese with English abstract).
Wei, G.F., Nie, J.T., Xin, H.G., Jiang, X.D., Zhang, Z.G., Yuan, S.C., 2005. Geological characteristics and regularity of gold enrichment of north ore-controlling ductile shear zone in Huachanggou gold deposit. J. Earth Sci. Environ. 27, 38–44 (in Chinese with English abstract).
Wen, B., Chen, M.S., Liu, X.Y., 2007. Ore-control factors and gold enrichment in the surroundings of the Baguamiao gold deposit. Northwest. Geol. 40, 37–43 (in Chinese with English abstract).
Xia, L.Q., Xia, Z.C., 1987. Some problems on the spilite–keratophyric volcanic rocks. Bulletion of Xi'an Institute of Geology and Mineral Resources. Chin. Acad. Geol. Sci. 19, 1–30 (in Chinese with English abstract).
Yang, T., Zhu, L.M., Zhang, G.W., Wang, F., Lu, R.K., Xia, J.C., Zhang, Y.Q., 2012a. Geological and geochemical constraints on genesis of the Liziyuan gold-dominated polymetal deposit, western Qinling orogen, central China. Int. Geol. Rev. 54, 1944–1966. http://dx.doi.org/10.1080/00206814.2012.704673.
Yang, X.A., Liu, J.J., Cao, Y., Han, S.Y., Gao, B.Y., Wang, H., Liu, Y.D., 2012b. Geochemistry and S, Pb isotope of the Yangla copper deposit, western Yunnan, China: implication for ore genesis. Lithos 144–145, 231–240. http://dx.doi.org/10.1016/j.lithos.2012.04.008.
Yin, A., Nie, S., 1996. A Phanerozoic palinspastic reconstruction of China and its neighboring regions. In: Yin, A., Harrison, T.M. (Eds.), The Tectonics of Asia. Cambridge University Press, New York, pp. 442–485.
Zartman, R.E., Doe, B.R., 1981. Plumbotectonics—the model. Tectonophysics 75, 135–162. http://dx.doi.org/10.1016/0040-1951(81)90213-4.
Zeng, Q.T., McCuaig, T.C., Hart, C.J.R., Jourdan, F., Muhling, J., Bagas, L., 2012. Structural and geochronological studies on the Liba goldfield of the West Qinling Orogen, Central China. Mineral. Deposita 47, 799–819. http://dx.doi.org/10.1007/s00126-011-0398-8.
Zhai, X.M., Day, H.W., Hacker, B.R., You, Z.D., 1998. Paleozoic metamorphism in the Qinling orogen, Tongbai Mountains, central China. Geology 26, 371–374. http://dx.doi.org/10.1130/0091-7613(1998)026<0371:PMITQO>2.3.CO;2.
Zhang, X.M., Spry, P.G., 1994. Petrological, mineralogical, fluid inclusion, and stable isotope studies of the Gies gold-silver telluride deposit, Judith Mountains, Montana. Econ. Geol. 89, 602–627. http://dx.doi.org/10.2113/gsecongeo.89.3.602.
Zhang, F.X., Wang, L.S., 2013. Exploration and research review of Carlin and Carlin-like type gold deposits in Qinling Mountains Orogenic belt. Gold Sci. Technol. 21, 21–27 (in Chinese with English abstract).
Zhang, L.G., Chen, Z.S., Liu, J.X., Yu, G.X., Wang, K.F., Wang, B.C., Xu, J.F., Zheng, W.S., Li, D.Y., Li, H., Hou, D.Y., 1995. Two-stage Water–Rock Isotopic Exchange Theory and Implied on Prospecting. Geological Publishing House, Beijing, pp. 19–21 (in Chinese with English abstract).
Zhang, Z.Q., Zhang, G.W., Tang, S.H., Xu, J.F., Yang, Y.C., Wang, J.H., 2002. Age of Anzishan granulites in the Mianxian–Lueyang suture zone of Qingling orogen: with a discussion of the timing of final assembly of Yangtze and North China craton blocks. Chin. Sci. Bull. 47, 1925–1930. http://dx.doi.org/10.1360/02tb9420.
Zhang, C.L., Gao, S., Yuan, H.L., Zhang, G.W., Yan, Y.X., Luo, J.L., Luo, J.H., 2007a. Sr–Nd–Pb isotopes of the Early Paleozoic mafic–ultramafic dykes and basalts from South Qinling belt and their implications for mantle composition. Sci. China Ser. D 50, 1293–1301. http://dx.doi.org/10.1007/s11430-007-0088-7.
Zhang, X.L., Chen, Y.R., Xu, H.Q., Tai, Y.H., Gui, S.H., 2007b. Matter source of the Huachanggou gold deposit in Shannxi province. Miner. Resour. Geol. 21, 17–21 (in Chinese with English abstract).
Zhang, L., Yang, R.S., Mao, S.D., Lu, Y.H., Qin, Y., Liu, H.J., 2009. Sr and Pb isotopic feature and ore-forming material source of the Yangshan gold deposit. Acta Petrol. Sin. 25, 2811–2822 (in Chinese with English abstract).
Zhang, S.H., Tang, S.H., Tang, D.Z., Pan, Z.J., Yang, F., 2010. The characteristics of coal reservoir pores and coal facies in Liulin district, Hedong coal field of China. Int. J. Coal Geol. 81, 117–127. http://dx.doi.org/10.1016/j.coal.2009.11.007.
Zhang, L., Liu, Y., Li, R.H., Huang, T., Zhang, R.Z., Chen, B.H., Li, J.K., 2014. Lead isotope geochemistry of Dayingezhuang gold deposit, Jiaodong Peninsula, China. Acta Petrol. Sin. 30, 2468–2480 (in Chinese with English abstract).
Zheng, Y.F., 1990. Carbon–oxygen isotopic covariation in hydrothermal calcite during degassing of CO_2: a quantitative evaluation and application to the Kushikino gold mining area in Japan. Mineral. Deposita 25, 246–250. http://dx.doi.org/10.1007/BF00198993.
Zheng, Y.F., Chen, J.F., 2000. Stable Isotope Geochemistry. Science Press, Beijing, pp. 1–316 (in Chinese).
Zheng, Y.F., Hoefs, J., 1993. Carbon and oxygen isotopic covariations in hydrothermal calcites. Mineral. Deposita 28, 79–89. http://dx.doi.org/10.1007/BF00196332.
Zheng, J.P., Griffin, W.L., Sun, M., O'Reilly, S.Y., Zhang, H.F., Zhou, H.W., Xiao, L., Tang, H.Y., Zhang, Z.H., 2010. Tectonic affinity of the west Qinling terrane (central China): North China or Yangtze? Tectonics 29, TC2009. http://dx.doi.org/10.1029/2008TC002428.
Zhou, Z.J., Qin, Y., Lin, Z.W., Wang, L.X., Wang, Z.Q., 2011a. Study of fluid inclusion characteristic and genetic type of the Huachanggou gold deposit, West Qinling Orogen. Acta Petrol. Sin. 27, 1311–1326 (in Chinese with English abstract).
Zhou, Z.J., Qin, Y., Lin, Z.W., 2011b. Study of C–H–O–S isotope of the Huachanggou gold deposit, West Qinling Orogen. Acta Mineral. Sin. 31, 678–679 (in Chinese with English abstract).
Zhou, Z.J., Lin, Z.W., Qin, Y., 2014. Geology, geochemistry and genesis of the Huachanggou gold deposit, western Qinling Orogen, central China. Geol. J. 49, 424–441. http://dx.doi.org/10.1002/gj.2557.
Zhu, B.Q., 1998. The Theory and Application of the Isotopic Systematic in Geoscience–Concurrent Discussion of the Continental Crust and Mantle Evolvement in China. Science Publishing House, Beijing, pp. 1–330 (in Chinese with English abstract).
Zhu, L.M., Zhang, G.W., Lee, B., Guo, B., Gong, H.J., Kang, L., Lv, S.L., 2009. Zircon U–Pb dating and geochemical study of the Xianggou granite in the Ma'anqiao gold deposit and its relationship with gold mineralization. Sci. China Ser. D Earth Sci. 39, 700–720 (in Chinese with English abstract).
Zhu, L.M., Zhang, G.W., Lee, B., Guo, B., Gong, H.J., Kang, L., Lü, S.L., 2010. Zircon U–Pb dating and geochemical study of the Xianggou granite in the Ma'anqiao gold deposit and its relationship with gold mineralization. Sci. China Earth Sci. 53, 220–240. http://dx.doi.org/10.1007/s11430-009-0100-5.